NOTICE

CERTAIN DATA CONTAINED IN THIS DOCUMENT MAY BE DIFFICULT TO READ IN MICROFICHE PRODUCTS.

DOE/PC/79676-T2
(DE91004166)

LIGHTWEIGHT TRANSFORMER

Final Report for the Period September 1987—May 1990

May 1990

Work Performed Under Contract No. AC22-87PC79676

For
U.S. Department of Energy
Pittsburgh Energy Technology Center
Pittsburgh, Pennsylvania

By
Avco Research Laboratory, Inc.
Everett, Massachusetts

DISCLAIMER

This report has been reproduced directly from the best available copy.

Available to DOE and DOE contractors from the Office of Scientific and Technical Information, P.O. Box 62, Oak Ridge, TN 37831; prices available from (615)576-8401, FTS 626-8401.

Available to the public from the National Technical Information Service, U. S. Department of Commerce, 5285 Port Royal Rd., Springfield, VA 22161.

Printed in the United States of America. Office of Scientific and Technical Information, Oak Ridge, Tennessee

DOE/PC/79676--T2

DE91 004166

LIGHTWEIGHT TRANSFORMER

Daniel W. Swallom and George Enos

Final Report for the Period September 1987 - May 1990

May 1990

prepared for

U.S. DEPARTMENT OF ENERGY
PITTSBURGH ENERGY TECHNOLOGY CENTER
Contract No. DE-AC22-87PC79676

by

AVCO RESEARCH LABORATORY, INC.
a subsidiary of Textron Inc.
2385 Revere Beach Parkway
Everett, Massachusetts 02149

FOREWORD

This final report was submitted by Avco Research Laboratory, Inc. under Contract No. DE-AC22-87PC79676. The effort was sponsored by the United States Department of Energy, Pittsburgh Energy Technology Center, Pittsburgh, Pennsylvania 15236, with Leo Makovsky as the Program Manager. The work discussed in this report was performed by Avco Research Laboratory, Inc., under the direction of George Enos, and by a major subcontractor, J. Busek Co., Inc., Needham, Massachusetts, under the direction of Dr. Vladimir J. Hruby.

The technical work performed on this contract consisted of the design, fabrication, and testing of a lightweight transformer. Avco Research Laboratory, Inc. conducted the overall program and performed the high power transformer tests. J. Busek Co., Inc. designed and fabricated the transformer and performed the low power testing.

This report was written and edited by the named authors of Avco Research Laboratory, Inc. and by Dr. Vladimir J. Hruby of J. Busek Co., Inc.

TABLE OF CONTENTS

LIST OF ILLUSTRATIONS

LIST OF TABLES

1.0 EXECUTIVE SUMMARY

The creation of the Strategic Defense Initiative Organization (SDIO) in 1983 has established a challenge to the technical community to provide the required science and engineering necessary to achieve the objectives of the SDIO. This technical challenge is present in the requirements for minimum mass, high performance power conditioning systems capable of achieving the space-based SDIO mission applications. Transformers and their related structure are major components of the power conditioning systems for many of the SDIO mission applications.

The technical effort described in this report relates to the program that was performed to design, fabricate, and test a lightweight transformer for SDIO mission requirements. The objectives of this program were two-fold: (1) design and fabricate a lightweight transformer using liquid hydrogen as the coolant; and (2) test the completed transformer assembly with a low voltage, dc power source. Although the full power testing with liquid helium was not completed, the program demonstrated the viability of the design approach. The lightweight transformer was designed and fabricated, and low and moderate power testing was completed. Thus, this approach to the design and fabrication of a lightweight transformer for a power conditioning system appears to be feasible.

The transformer designed during this program is a liquid hydrogen cooled air core transformer that uses thin copper for its primary and secondary windings. The transformer winding mass was approximately 12 kg, or 0.03 kg/kW. Further refinements of the design to a partial air core transformer could potentially reduce the winding mass to as low as 4 or 5 kg, or 0.0125 kg/kW. No attempt was made on this program to reduce the mass of the related structural components or cryogenic container.

While the results obtained during the program did not fully achieve the initial program goals, the program successfully demonstrated the lightweight transformer concept. A short between the transformer windings occurred during the preparations for the final test. This prevented any further testing of the transformer. Based on the results obtained, this transformer technology shows promise for substantially reducing the transformer mass, and further development and refinement of this concept should be pursued.

2.0 INTRODUCTION

The long range plans of both the National Aeronautics and Space Administration (NASA) and the Department of Defense (DOD) for future missions in space include the need for large electrical power systems in the megawatt-level range. These power systems will, of course, require suitable megawatt-level inverter/converter systems to deliver the power to the electrical load at the proper voltage and current levels. Thus, a power conditioning system must be developed in concert with the power requirements as well as the specific electrical load requirements.

The most massive components of the power conditioning system are the nonelectrical, structural components and the power transformer. Estimates show that about eighty percent of the mass of a megawatt or larger dc to dc converter is comprised of the transformer plus the structural, insulating, and cooling components. Nearly half of that mass is the transformer. Thus, a substantial reduction of the transformer mass would allow a similar reduction in the structural components, and therefore, would have a significant impact on the mass of the power conditioning system. Hence, the focus of this technical effort is on the development of a lightweight transformer.

An air core, cryogenically cooled transformer can achieve the desired mass reduction. Approximate calculations indicate that the cryogenic, air core transformer is nearly an order of magnitude less massive than the conventional design with a ferromagnetic core. This may lead to an estimated 50 percent mass reduction of the power conditioning system. The cryogenic fluid is liquid hydrogen, which is already required in large quantities by most of the space-based electrical loads under consideration. Thus, neither the liquid hydrogen consumption nor the complexity of the system is appreciably impacted by a cryogenic transformer.

Low voltage dc generators are being considered as power sources for space-based NASA and DOD mission applications. A study of the feasibility of various power sources and their respective architectures for a variety of DOD applications was recently completed. This study, the Space Power Architecture Study, was performed by Martin Marietta and evaluated the prospective power sources for a variety of electrical loads.[1] The study evaluated both directed energy (DEW) and kinetic energy weapons (KEW) that would require substantial amounts of electrical power. All of these devices require multimegawatt dc power. With the exception of the electromagnetic launcher, the remaining weapons require 100 kV dc or higher input voltages. Thus, these DEW systems require a multimegawatt power conditioning system for nearly every potential combination of power source and weapon.

For space applications, the power conditioning system mass, volume, and efficiency are of critical importance. Based on current technology, an analysis of the space-based 1 MW dc to dc converter switched at 5 kHz with 5 kV dc input and 100 kV dc output indicates the following mass distribution.[2]

	m (kg)	Percent
Semiconductors	30	5.4
Filters (inductors and capacitors)	55	10 0
Transformer	157	28.6
Mechanical (Structural, Thermal and Insulating Components	308	56.0
	550	100.0

Thus, the mechanical packaging and the transformers, which are a necessary part of any power conditioning system, represent about 80 percent of the total mass of the dc to dc converter.

To reduce the "mechanicals", the design must depart from the standard established practices and integrate the many previously separate structural, insulating, and cooling components into fewer multirole components: hence, the result is a lighter system. The highly thermally conductive, electrically insulating, mechanically strong materials, such as silicon nitride and beryllium oxide, can be used. These materials, which are both lighter than aluminum, offer significant potential for substantial mass reduction.

To reduce the mass of the transformers, the switching frequency can be increased (transformer mass is inversely proportional to the 0.5 to 0.75 power of its switching frequency) while utilizing the best available magnetic cores. An alternative and potentially more rewarding approach is to develop an "air core" transformer.

The switching frequency is limited by the available semiconductor switches. The practical limit for high power SCR switches is about 25 kHz. When these devices are connected in parallel and in series to achieve greater current and voltage handling capability, the maximum practical frequency is 5 kHz. Furthermore, above the 5 kHz switching frequency, studies have shown that high voltage transformers cease to obey the inverse power law mass vs frequency relationship.(3) The transformer mass becomes nearly frequency independent above 10 kHz. Thus, to increase the frequency above 5 kHz is unproductive while at the same time the circuit losses are increased.

Because a lightweight transformer requires less structural support, the transformer mass reduction is amplified into a greater overall power conditioning mass reduction. A 50 percent power conditioning mass savings by using air core transformers appears possible. Hence, the use of multimegawatt, air core transformers could have a very significant impact on low voltage, space-based power systems, and they could be used in any low mass power conditioning system that couples any multimegawatt power source to its load.

The present concept evolved from investigating high power (100 MW_e), high output voltage (100 kV) cryogenic air core transformers as a lightweight alternative to the conventional iron core transformers.(2) A conventional/continuously operating air core transformer was shown to be as much as an order of magnitude lighter than the conventional alternative.

Air core transformers function in the same manner as transformers with magnetic cores. Two or more inductively coupled coils are wound on a mandrel so that when one coil is energized, the high rate of change of the generated magnetic flux produces voltage on the terminals of the other coil. Because of the absence of ferromagnetic or ferrite cores that provide a low impedance (high magnetic permeability) path for the magnetic flux in conventional transformers, low power, small size air core transformers that have self inductance comparable to their leakage inductance are therefore are not practical. Furthermore, because the flux linkage is strongly dependent upon the proximity of the windings of one coil to the windings of the other coil(s), the magnetic coupling is in general lower than in conventional transformers with magnetic cores. However, these disadvantages are mitigated in high power, high current, and high voltage applications where the interwinding spacing becomes small relative to the coil size, and the low permeability is offset by large coil cross-sectional area (winding radius). In addition, the absence of the core material makes the air core transformer free of current limits and core saturation limits. These attributes make the air core transformer well suited for high power (10^{10} watts), high primary current and secondary voltage (megavolts), short duration (microseconds) pulsed applications.[4] Short pulse and low rep rate means low energy transfer that permits the transformer to operate in a heat sink mode. The salient innovative feature of the present design is its continuous operation, which is permitted by cryogenic cooling. These transformers could then be used in any application from pulse mode to continuous duty without the usual limit of the joule heating transformer winding losses. The transformer could be used in any power conditioning circuit, inserted between any power source and load combination. Thus, its applicability is universal and not limited to a specific power system.

The most common type of an air core transformer has spiral windings made of thin and wide conductor sheets separated by a wider insulating sheet as shown in Figure 1. The inner winding is usually the secondary and the outer is the primary. This practice was followed in the transformer designed and constructed during this effort.

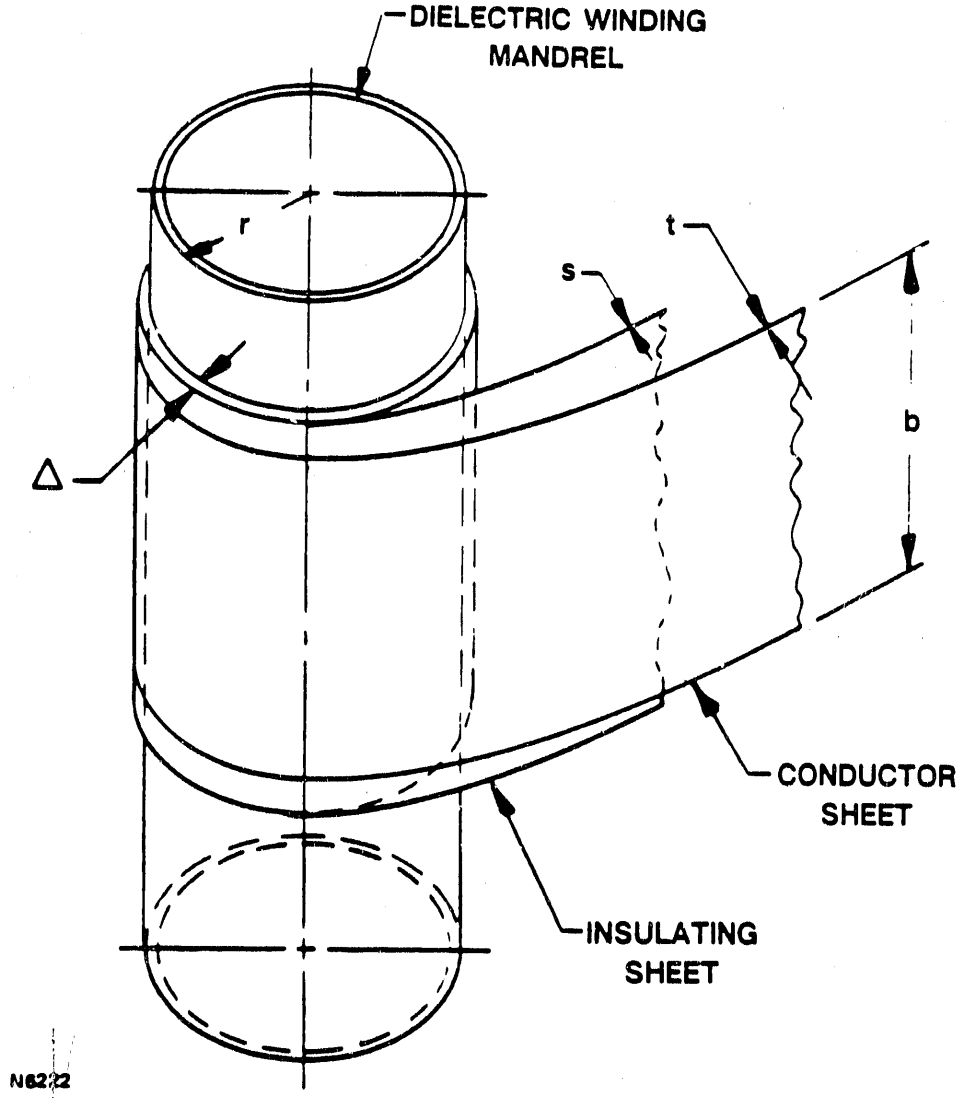

Figure 1 Schematic of Spiral Wound Air Core Transformer

3.0 TRANSFORMER DESIGN

The overriding factors in the design of the transformer were determined by the available test equipment and by the requirement to make the experimental design scalable to actual large power transformers. The existing equipment included:

1. Set of semiconductor switching circuits
2. DC power supply
3. Water-cooled load

Because of the nature of the switching circuit and its operating frequency the experimental transformer had to have a mid-tap primary and operate at 1 kHz. The power supply and the load voltage rating dictated the maximum transformer voltage ratio of ten and a maximum power transfer of 400 kWe. These parameters were then selected to be the basic inputs into the design process and the traditional approach to the air core transformer winding structure (a spiral with foil type conductor as shown in Figure 1) was adopted. Several conceptual design geometries (i.e., diameter and winding width) were evaluated to determine those with the smallest winding mass. Two designs were selected to be carried to the next step - the engineering design. The mass of the structural components was not an issue that was addressed in this proof-of-concept program.

There are three distinct transformer design considerations. The foremost is electrical, followed by mechanical and thermal. Each is discussed in the following paragraphs.

3.1 ELECTRICAL DESIGN

The two designs that were selected differ in conductor current density and average core permeability. The salient specifications are shown in Table 1. A 50 percent increase in current density and an increase in permeability (from pure air core to a core with a ferromagnetic foil) results in conductor mass reduction from about 12 kg to 4 kg. This substantial mass reduction provided the incentive to perform the detailed engineering designs for both transformers. The overall assembly of both designs is shown in Figures 2a and 2b. The relative sizes can be compared using this figure.

In order to rapidly evaluate many potential designs, a spread sheet based design procedure was written. The inputs are:

1.	Transformer primary current	I_p (A)
2.	Transformer primary voltage	V_p (volts)
3.	Half the switching period	Δt (sec)
4.	Conductor current density	J (A/m^2)
5.	Thickness of the conductor foil	t_p, t_s (m)
6.	Thickness of the insulator foil	S_p, S_s (m)
7.	Winding width of radius ratio	b/r
8.	Turn ratio	N_p/N_s
9.	Magnetizing to primary current ratio	I_m/I_p
10.	Conductor and insulator density	P_c, P_s (kg/m^3)
11.	Conductor resistivity	P_R (Ω-m)
12.	Conductor and insulator heat capacity	C_c, C_s (Joules/kg - K)

With these inputs plus relative permeability and permittivity, the procedure is used to evaluate a set of equations that constitute the electrical design of the transformer.

The winding width, b, and winding radius, r, are calculated from the inputs, I_p, J_p, and t_p. The required primary inductance, L_p, to sustain the primary voltage for the given time for a foil wound coil is given by

$$L_p = \frac{V_p \Delta t}{I_m (1 + r/b)}. \quad (1)$$

The number of primary turns (N_p) is

$$N_p = \sqrt{\frac{L_p (1 + b/r)}{\pi \mu_o r}}, \quad (2)$$

TABLE 1

SALIENT DESIGN PARAMETERS OF THE LIGHTWEIGHT TRANSFORMER

Design		Baseline Design	High Risk Design
Current (I_p)	A	4000	4000
Voltage (V_p)	V	100	100
Current Density (J)	A/m^2	2×10^8	3×10^8
Permeability ($\mu_{effective}$)	-	1	3
Conductor	-	Cu 101/Cryo Grade	Cu 101/Cryo Grade
Insulator	-	KAPTON	KAPTON
Winding width/radius ratio (b/r)	-	0.9	1.0
Radius (r)	m	0.219	0.131
Number of turns-primary (N_p)	-	11.4	9.0
Number of turns-secondary (N_s)	-	114	90
Conductor Mass (m_{total})	kg	11.92	4.1
Efficiency (η_T)(±)	-	98.4	98.8
LH_2 Mass (m_{LH2})	kg/s	0.125	0.088
Pressure Drop (Δp)	atm	0.563	0.774
Design Number	10		
Winding power density	kW/kg	0.03	0.01

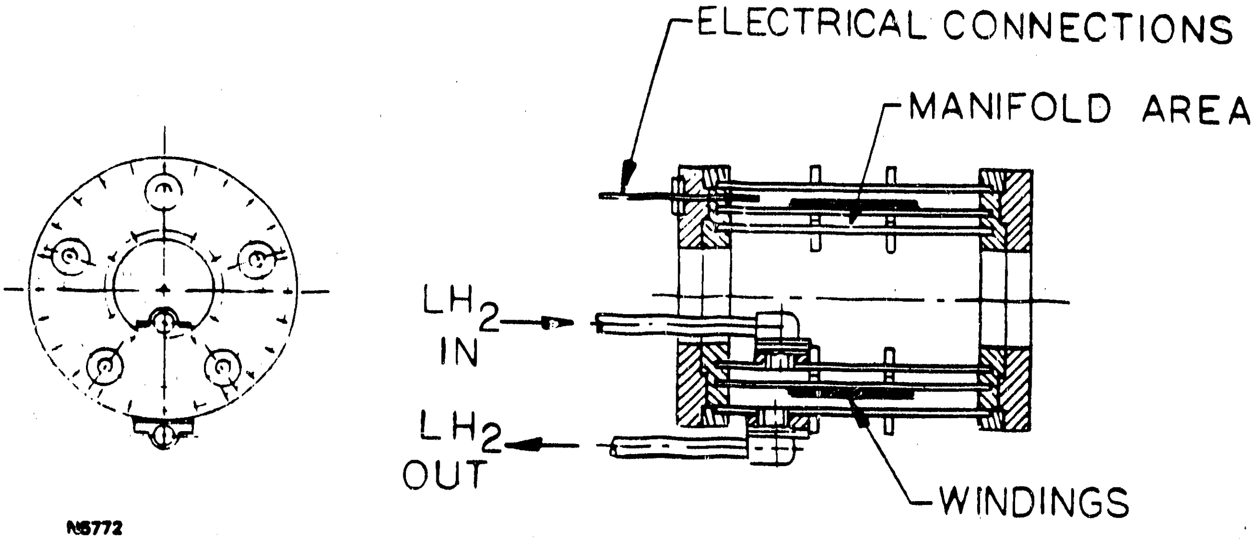

Figure 2a Overall Assembly of Baseline Design No. 17

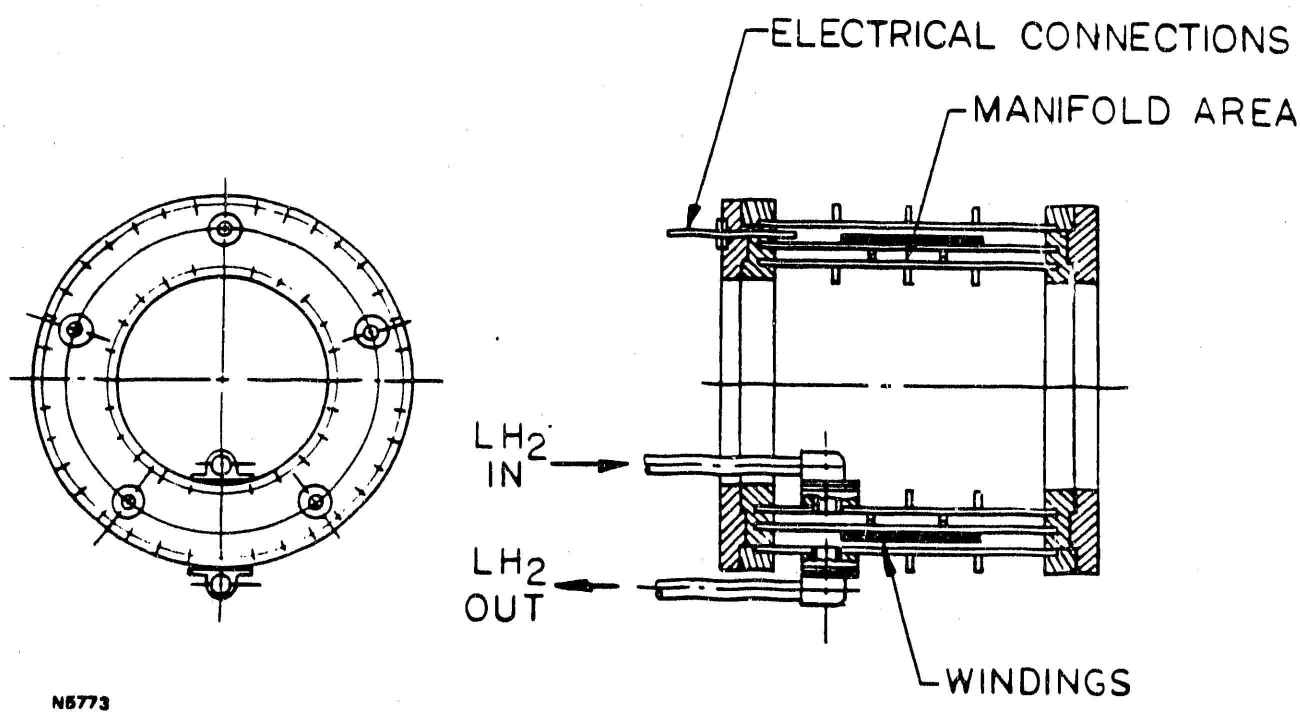

Figure 2b Overall Assembly of High Risk Design No. 10

where μ_o and μ_r are absolute and relative magnetic permeabilities. The number of secondary turns is calculated from the given turn ratio and N_p. The leakage inductance, L', is given by:

$$L' = \frac{2}{3} \pi \Delta \mu_o \left(\frac{b}{r}\right) N_p^2 \quad , \tag{3}$$

where $\Delta = 2 N_p (t_p + S_p) + N_s (t_s + S_s)$ = total winding radial thickness. The factor of two is needed to account for the center tapped primary because N_p is the number of turns on one side of the center tap only. The recommended practice is to exclude partial turns in any transformer; this practice has been followed in this design as well. Because the primary is center tapped, the total number of turns is 23 with the center tap at 11.5 turns. This minimizes the departure from the calculated value of 11.4 turns.

The mutual inductance, M, was calculated using the modified Nagaoka formula.[5] Under a restricted set of circumstances, the formula can be expressed in the form of a series as shown below.

$$M = 0.002 \frac{\pi^2 a^2 N_1 N_2}{\rho} \left\{ 1 - \frac{1}{2} \left(\frac{A}{\rho}\right)^2 B \left[\lambda_2 + \lambda_4\, {}_2B + \lambda_6\, {}_4B^2 + \lambda_8\, {}_6B^3 \ldots\right] \right\} \tag{4}$$

where

a	=	mid radius of the inner (secondary) coil
A	=	mid radius of the outer (primary) coil
$N_{1,2}$	=	Number of turns of the secondary and primary windings
ρ^2	=	$a^2 + (b/2)^2$
δ^2	=	$A^2 + (b/2)^2$
B	=	$(\delta/\rho)^2$, $\gamma = (a/\delta)^2$
λ_2	=	$1 - 7/4\ \gamma$
λ_4	=	$1 - 9/2\ \gamma + 33/8\ \gamma^2$
λ_6	=	$1 - 33/4\ \gamma + 143/8\ \gamma^2 - 715/64\ \gamma^3$
λ_8	=	$1 - 13\ \gamma + 195/4\ \gamma^2 - 1105/16\ \gamma^3 + 4199/128\ \gamma^4$

The coefficients ξ_{2n} are the same functions of $(A/\rho)^2$ as λ_{2n} are of $\gamma = (a/\delta)^2$, e.g., $\xi_2 = 1 - 7/4\ (A/\rho)^2$, etc.

The series converges slowly when the outer and the inner coils have the same width (b), which is the present case. However, it has been used successfully before and gives satisfactory results.

The mutual inductance, M, was calculated using the above equation, and the primary and the secondary inductances were calculated using the equation:

$$L = \frac{\rho \pi r N^2}{(1 + b/r)} . \tag{5}$$

The magnetic coupling coefficient k was calculated as:

$$k = M/\sqrt{L_p L_s} \tag{6}$$

where L_p and L_s are the primary and secondary self inductances.

For the design No. 17, the coupling coefficient exceeded the theoretical maximum of $k = 1$ and was calculated to be $k = 1.003$. This error was attributed to the inaccuracy of the series expression for M.

The calculations were used to evaluate the pulse rise time, pulse droop, magnetic pressure on the coil, peak magnetic field, resistance of each coil, power losses, insulation stress, length of conductors and insulators. Also calculated is the transformer temperature rise if left uncooled.

The designs are evaluated on the basis of acceptable pulse rise time, droop, insulation stress and mass of the winding.

The principal difficulty with any air core design is to minimize the leakage inductance while maximizing the self inductance. This difficulty is overcome by minimizing the interwinding distances, which requires the conductor and the insulator to be as thin as possible and to interleaf the primary with the secondary windings. Aluminum and copper foils/conductors were considered and copper was selected because of its slightly better electrical conductivity and because it is not as sensitive to work hardening as aluminum. Because the transformers step up voltage by a factor of 10, the secondary foil/conductor having the same width and current density as the primary foil must be 10 times thinner. Availability dictated the minimum foil thickness to be about 0.0004". The minimum available insulator thickness (Kapton) is 0.013 mm. These dimensions were then selected as the baseline.

The possibility of metalizing the Kapton and using the metalized layer as the secondary conductor was also considered. This metalized insulating fiber technique is being applied to high energy capacitors with reasonable success. However, no experience exists with this material combination at cryogenic temperature. The primary concern for this combination was the differential thermal expansion of the metalized layer and the substrate which would most likely lead to breakages in the metalized layer and its separation from the substrate. Furthermore, the separated flakes of metal could cause cooling flow blockage. Because of these potential problems, this "metalization" approach was not pursued further. However, the promise of this approach appears to warrant future investigation.

3.2 MECHANICAL AND THERMAL DESIGN

The transformer cannot be sufficiently cooled by submersion into a LH_2 bath. Therefore, a flow through system was devised. Figures 2, 3, and 4 illustrate the packaging and cooling approach. The structure consists of three concentric pipes flanged on both ends, and the material is cryogenic grade G10. The space between the innermost pipe and the middle pipe (the winding mandrel) serves as the LH_2 manifold.

The initial approach was to wind the secondary coil first and after an appropriate number of turns, the primary would be interwound into the secondary. The two would then be wound together. At midpoint of the primary, the mid-tap would be added. Both windings then would terminate at the outside diameter of the coil. Because of cooling considerations, both the primary and the secondary windings consist of two separate coils wound in parallel, while the insulator sheet spans both coils. The corrugated structure of the insulator sheet is shown in a detailed view in Figure 3 and is not shown in Figure 4 for clarity. However, because of the difficulty of winding the thin secondary conductor prevented the primary/secondary interleafing, the primary was wound on top of the completed secondary.

The LH_2 flows from the manifold through a set of radial holes in the mandrel and through perforations in the Kapton sheets into the interwinding spaces created by the corrugated structure. In this manner, the LH_2 is in direct contact with approximately 50 percent of each turn of the conductor.

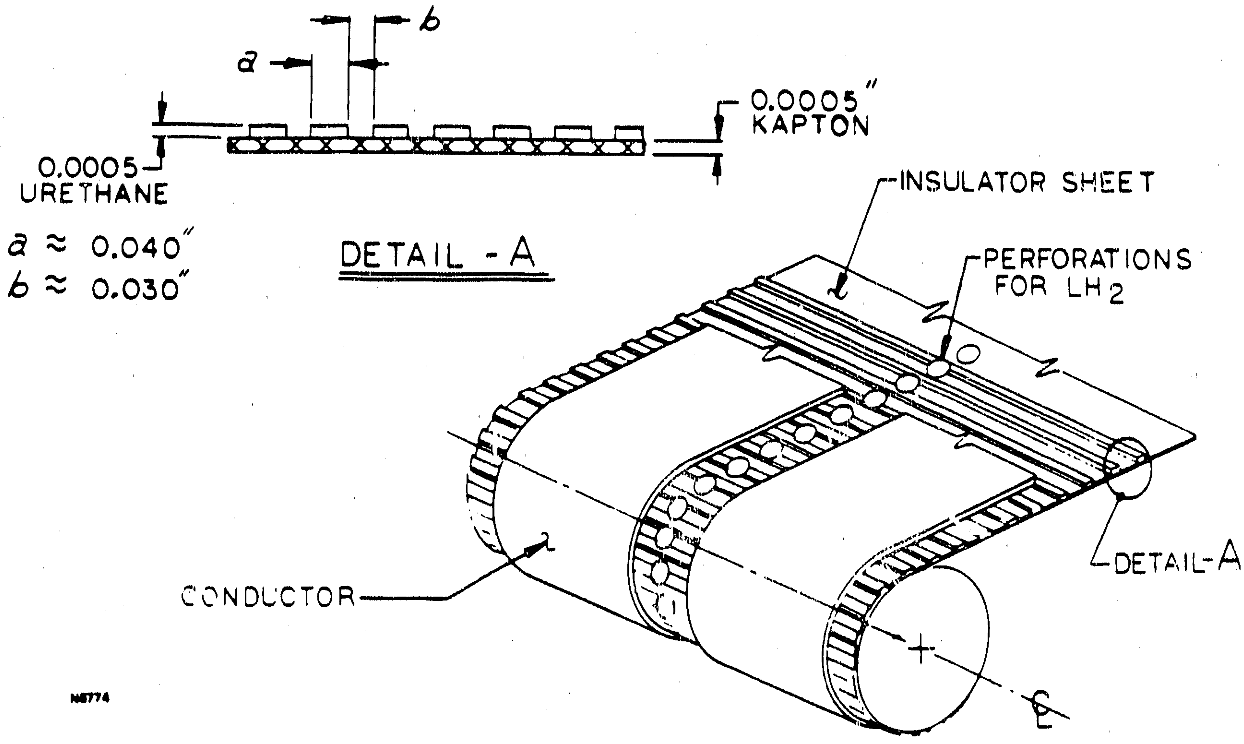

Figure 3 3-D Schematic of Winding

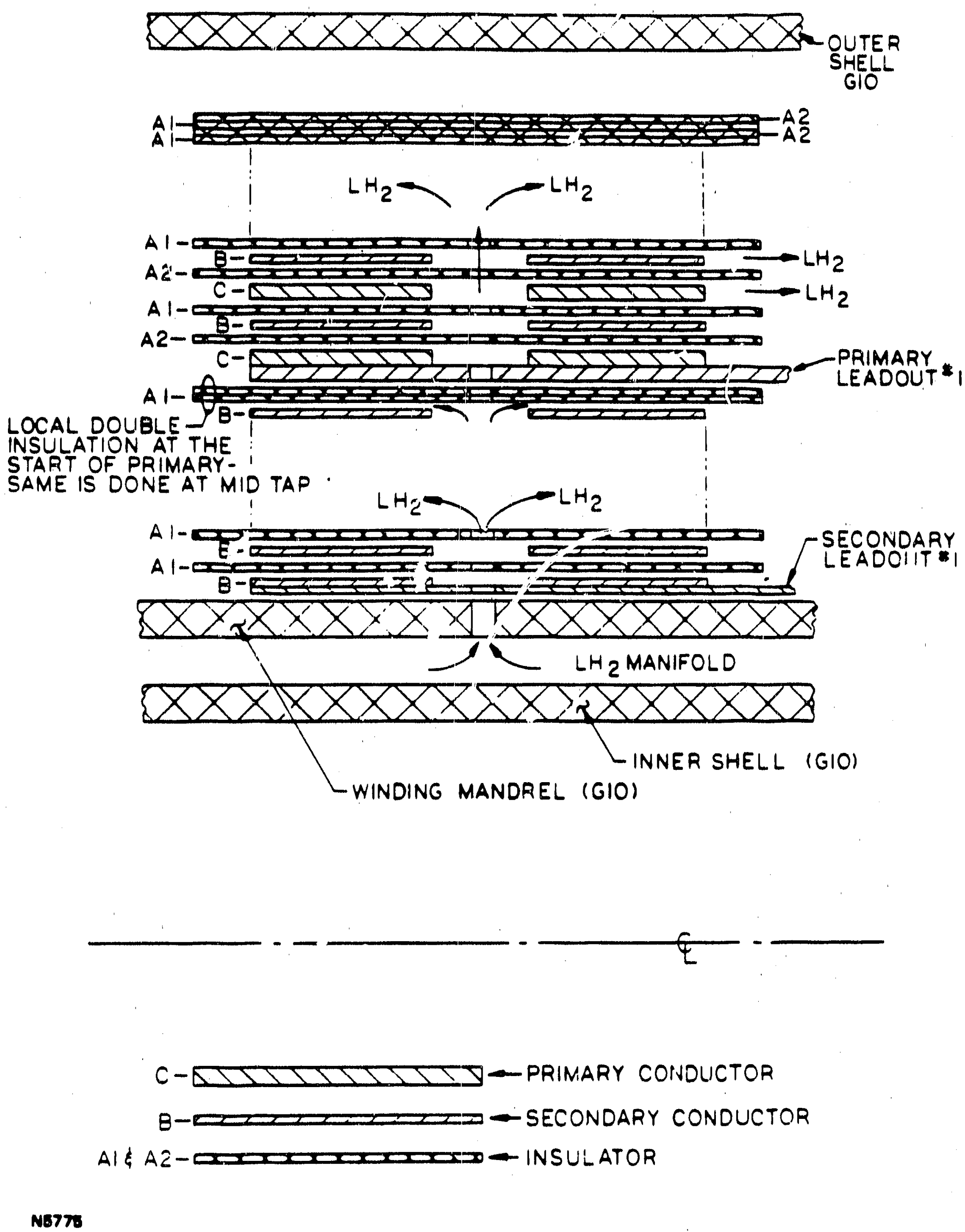

Figure 4 Cross Sectional Schematic of Layered Winding

It then exits the winding on both ends of the coils and fills the space between the mandrel and the outermost pipe. Subsequently, it exits through the discharge port and the tubular electrical connections shown in Figure 2a.

One of the most difficult engineering design problems was to seal the liquid and gaseous hydrogen. Normally, the 20 K liquid is sealed in metallic containers that are either welded or flanged with the seal provided by metallic O-rings. In the present application, no continuous electrically conducting loop that intercepts the transformer magnetic flux can be permitted. Such a loop would experience induced electric currents with corresponding heating, loss of the LH_2 metallic O-ring seal, and degradation of transformer performance. Thus, the material to be used for sealing in place of metal is polychlorotrifluoroethylene (CTFE).

The method of corrugation of the insulator sheets underwent several changes. The approaches investigated included drawing lines or printing the lines using urethane paint on one side of the Kapton. A drafting type computer plotter was adapted for this purpose.

The interwinding LH_2 velocity, flow rate, liquid quality, heat transfer coefficients, and pressure drop of the LH_2 coolant were calculated by using the spread sheet procedure mentioned above. Some of these results are included in Table 1. The methods employed to perform these calculations are discussed below.

The LH_2 channels and their dimensions are schematically shown in Figure 5. Two constraints must be placed on their geometry. The first constraint is the spacing between the strips, W_g, and the height of the strip, h_s. It must be such that the minimum height of the LH_2 channel, h_{min}, is approximately equal to h_s. The h_{min} is defined by a straight line between the corners of neighboring strips. A pliable material wound on top of these strips would span the LH_2 channel in this manner. Should h_{min} be allowed to become substantially smaller than h_s, the flow passage would be substantially blocked off. For this reason, h_{min}/h_s has been selected to be 0.9.

The second constraint is the gap width, W_g, relative to the width of the strip. If $W_g > W_s$, the strips in the next turn could "fall" into the gaps of the underlying turn and again block off the flow. The strips must be wider than the spacing between them. However, in order to maximize the heat transfer area of the copper conductor to LH_2, the strips should be as narrow as possible. The ratio of W_g/W_s was selected to be 0.75.

With these two constraints and the equation below (formed by applying purely geometrical arguments), the width of the strip can be calculated.

$$W_s = \frac{2r_1}{(1 + W_g/W_s)} \cos^{-1} \left\{ \frac{(h_{min}/h_s + r_1/h_s)}{(r_1/h_s + 1)} \right\} \qquad (7)$$

By applying typical r_1 = 25 cm and strip height of 0.025 mm to minimize the interwinding distance, the resulting W_s = 1.250 mm and correspondingly the gap would be $W_g \sim 1.0$ mm. The length of the secondary conductor in design No. 17 (low risk) is approximately 160 m. Thus, the required number of strips, corrugations shown in Figure 3, is 70,000. If all of these passages were filled with LH_2, approximately 3.5 sec would be required to boil off the LH_2 at full transformer power (4000 A and 100 V on the primary). By increasing the volume of these passages, the objective of this program, which is to operate the transformer for 10 seconds at full power, could be accomplished. However, the design would be very marginal. Therefore, a continuous duty design was selected for demonstration and the LH_2 was designed to flow through the transformer.

Two heat transfer processes occur within a cooling passage. One is convection. The second and more important is nuclei boiling. The heat transfer coefficient for laminar convection (h_e) is given by[6]

$$h_e = \frac{K}{(W_g + h_s)} \frac{(Re)(Pr)}{b/2D_h} \qquad (8)$$

where K is the thermal conductivity of LH_2, b is the length of the passage, D_h is its hydraulic diameter, Re and Pr are the Reynolds number (based on D_h) and Prandtl number, respectively.

The velocity necessary to determine the LH_2 consumption, pressure drop and the heat transfer rate was calculated as follows. First a passage volume and the heat flux imposed on the velocity was calculated. Then, the time to boil off this volume was determined; a third of this time was taken as the maximum allowable residence time. The time in turn determined the LH_2

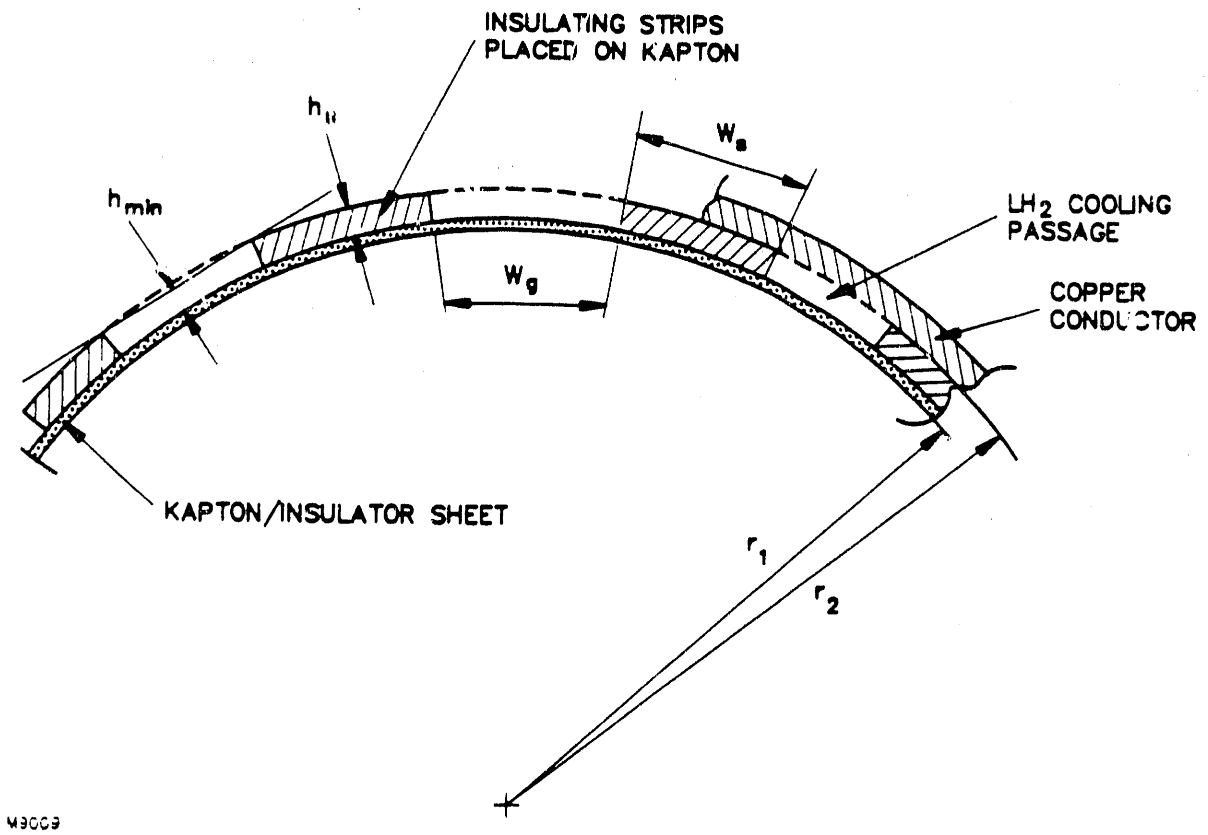

Figure 5 Geometry and Dimensions of the LH_2 Cooling Passages

velocity. This means that near the end of the cooling passage approximately 30 percent of the LH_2 has changed phase from liquid to gas.

The effective heat transfer coefficient for nuclei boiling is defined as

$$h_{nb} = \frac{Q/A}{\Delta T_b} \tag{9}$$

where the Q/A is the imposed heat flux per unit area of the passage and ΔT_b is the difference between the wall temperature and the LH_2 saturation temperature. The temperature difference is given by[6]

$$\Delta T_b = c_{sf} \frac{h_{fg}}{C_{pl}} Pr^{1.7} \left[\frac{Q/A}{\mu_e h_{fg}} \sqrt{\frac{1}{g} \frac{\sigma}{\rho_e - \rho_v}} \right]^{1/3} \tag{10}$$

where c_{sf} is a coefficient determined by the particular fluid solid surface combination. For this design the best estimate from the available data is $c_{sf} = 0.013$. The h_{fg} is the latent heat of vaporization, c_{pl} is the heat capacity of the liquid, μ_e is the viscosity of the liquid, ρ_e and ρ_v are the densities of the liquid and vapor, respectively, and σ is the surface tension of the liquid. The value of h_{nb} was calculated in this manner to compare its predicted value to the published data, and thereby determine the accuracy of the calculations.

The combined laminar and nucleate boiling heat transfer and the conductor surface temperature were calculated to insure that the conductor does not depart from the LH_2 temperature by more than 100 K. Should the temperature be allowed to rise above this limit, the conductor electrical conductivity starts rapidly decreasing which leads to more boiling and eventual burn out. The simple steady state calculations, of course, cannot handle this "runaway" regime so that the design criteria was selected to maintain $\Delta T_b < 50$ K. In fact both designs were held to ΔT_b below 0.6 K to ensure stable situation.

Two pressure drops, Δp, were calculated for each design case. The laminar flow pressure drop that would be expected to occur under unloaded transformer conditions and a two phase flow pressure drop that would occur with the transformer under full load. The laminar Δp is obviously insignificant relative to the phase flow Δp and is not be discussed. However, the Δp_{TPF} becomes especially important because the transformer is similar to a LH_2 boiler and must have adequate pressure relief margins to prevent explosions.

The two phase flow pressure gradient is calculated as

$$\left(\frac{\Delta p}{\Delta L}\right)_{TPF} = \left(\frac{\Delta p}{\Delta L}\right)_{Laminar} \Phi_e^2 \qquad (11)$$

where Φ_e is a function of a parameter X given by

$$X = \left(\frac{\rho_v}{\rho_e}\right)^{1/2} \left(\frac{\mu_e}{\mu_e}\right)^{0.125} \left(\frac{1}{x} - 1\right)^{0.875} \qquad (12)$$

where x is the vapor quality and the rest of the symbols were defined before. In order to make the calculations suitable for the spread sheet, the function of Φ vs X was digitized and fitted with an analytical function

$$\Phi = \coth X + 2.2 \left(\frac{1}{X}\right)^{0.6} \qquad (13)$$

The error over the range of interest was less than 5 percent. By using these relations, the pressure drop across the length of the package for both designs was calculated to be 0.57 and 0.78 atm, respectively.

4.0 TRANSFORMER MANUFACTURING

The transformer was wound on an in-house designed and constructed winding machine. The schematic of this machine is shown in Figure 6.

The construction of the transformer proceeded as follows:

1. The liquid hydrogen (LH_2) channels were deposited on an oversized (width wise) KAPTON sheet about 250 m long.
2. The KAPTON sheet was trimmed to width and perforated to allow LH_2 flow through the successive turns.
3. The secondary conductor was wound on a fiberglass double wall mandrel together with the KAPTON sheet insulator. (The space between the double walls serves as an LH_2 manifold.)
4. When the secondary was completed, it was banded with approximately three turns of KAPTON and bonded together with urethane.
5. The primary conductor was wound on top of the secondary by using the same KAPTON sheet with the LH_2 channels on it.
6. The whole assembly was banded together in the same manner as the secondary winding. The electrical leadouts from the winding were made by bending the foil conductors so as to bring the conductors outside of the winding where the foils were clamped between copper block terminals.
7. The completed winding was then inserted onto the outer shell. The top flange contained all the electrical and cryogen connections.

The salient details of this process are described below.

The LH_2 flows through all turns of the windings via a large number of microchannels as described in the previous section. The microchannels are formed on the KAPTON sheet by depositing urethane on that sheet. The geometry is shown in Figure 3. The urethane is deposited on the KAPTON from a specially adapted computer driven drafting plotter. The normal drafting pen was replaced by a pressurized syringe. A photo of the plotter installed on to the winding machine is shown in Figure 7. The details of the syringe connected to a urethane reservoir is shown in Figure 8. Great effort was expended to make this system work reliably and deposit consistent thickness,

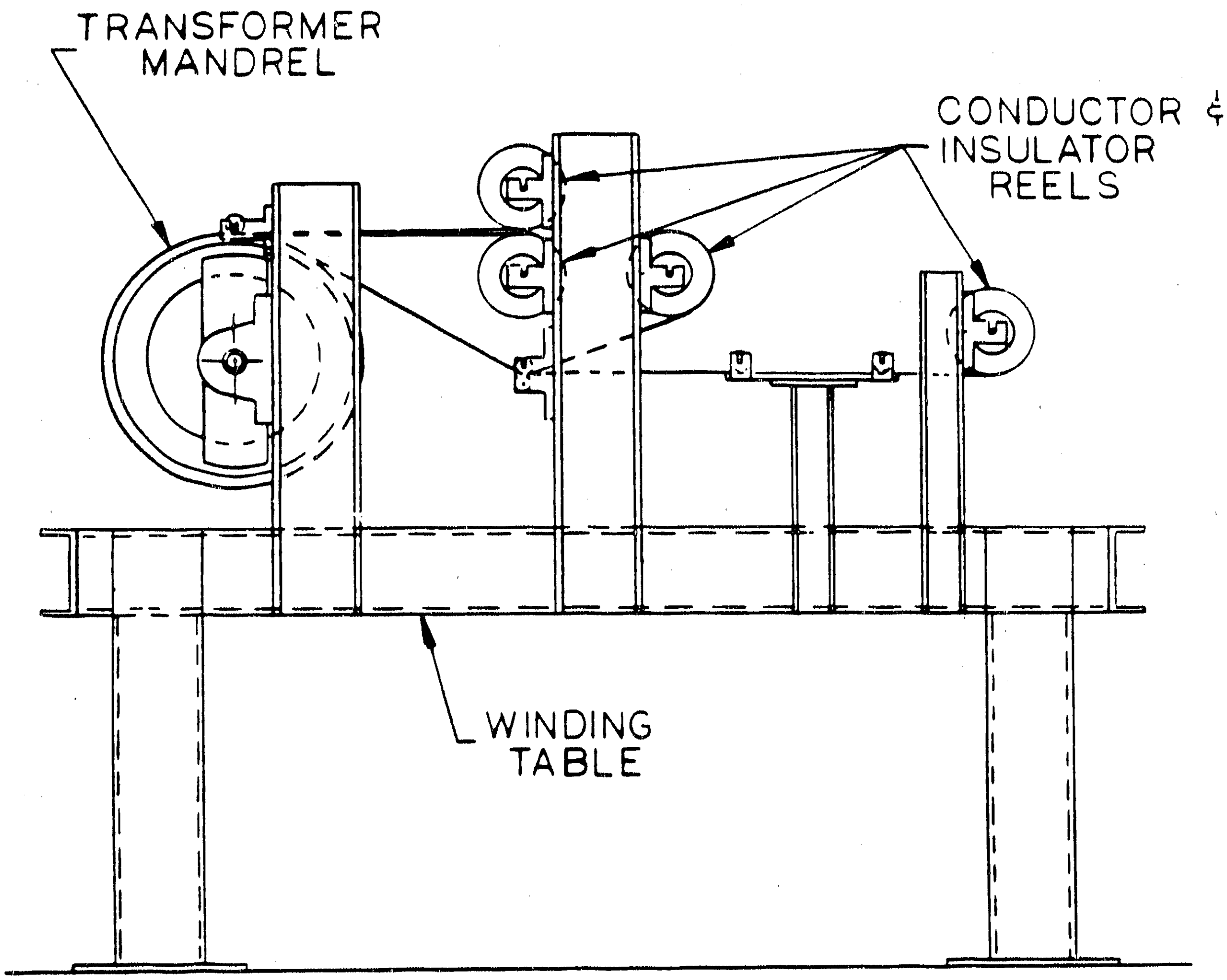

Figure 6 Schematic of the Winding Machine

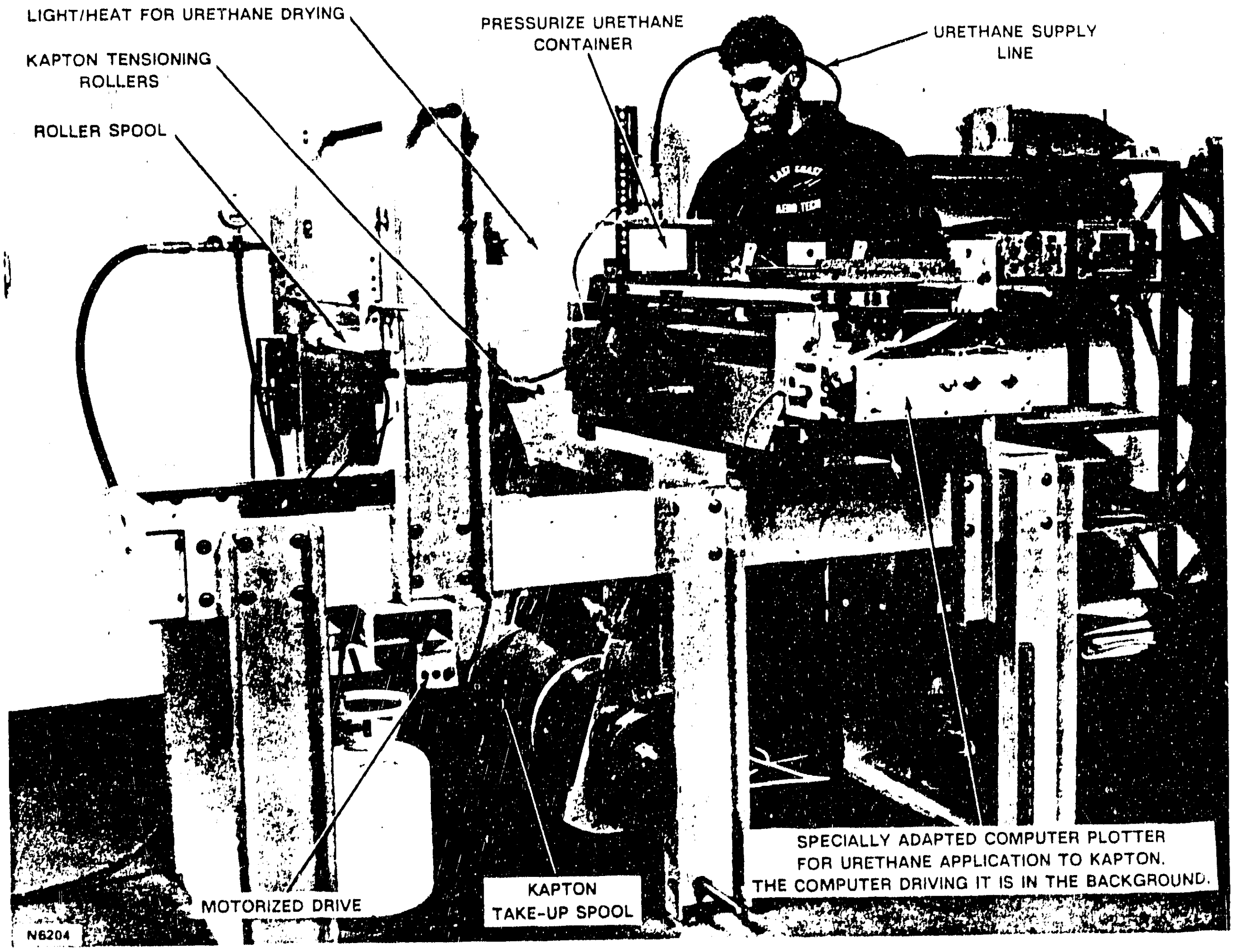

Figure 7   Air Core Transformer Winding Machine

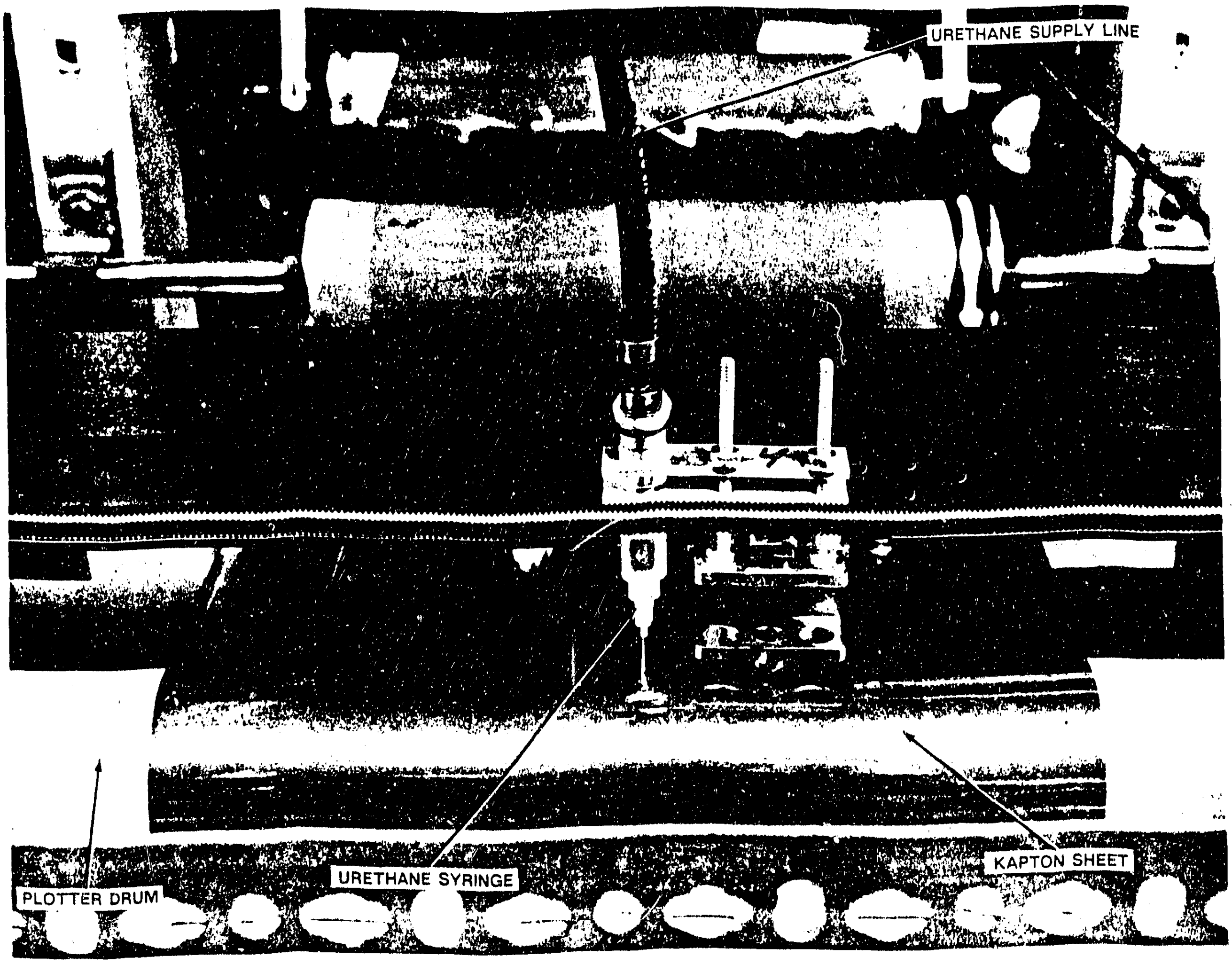

N6206

Figure 8 Close-Up of the Urethane/Syringe Drawing Urethane Lines on the Insulator Sheet (KAPTON) width and spacing of the urethane lines. A method was also worked out to dry the urethane before winding the KAPTON on a take-up spool. After this was accomplished, the system operated for six to eight hours a day for a total of 120 hours to draw approximately 120,000 lines on the 215 m long KAPTON sheet. Following this operation, the KAPTON sheet was trimmed to the desired width of 30 cm and perforated as shown schematically in Figure 9. This pattern ensures that every LH_2 channel receives its share of the coolant and that the holes overlap thus permitting the LH_2 to reach the outermost coil layers. The trimming and the perforation were done on a special fixture with the KAPTON rolled on a 27.3 cm diameter steel drum that was predrilled with the hole pattern shown in Figure 9. The drilling of the KAPTON was done by using a lubricated core-type drill.

Machined, cryogenic grade, laminated fiberglass (NEMA Grade G10) tubes and flanges were used for the transformer structure. First, the inner tube and the winding mandrel were glued to the manifold flanges. This assembly is shown in Figure 10. The adhesive was a cryogenic epoxy Crest No. 7450 A and B made by Crest Products. The tubes were also pinned to the flanges using G10 dowel pins for added structural strength. Reinforcing ribs were glued to both sides of the inner tube and to the inside diameter of the winding mandrel as indicated. Next, the outer tube with its reinforcing ribs was glued to its flanges. The winding mandrel subassembly was inserted into the outer tube, and the end flanges were placed on the top and bottom of the two subassemblies. These flanges were placed on the top and bottom of the two subassemblies and were pulled together with stainless steel threaded rods. This clamping aligned the outer flanges with the manifold flanges and ensured parallel surfaces for the "O" ring seals on the flanges. The glue joints were cured in this clamped assembly. After the glue joints were cured, the winding mandrel subassembly, consisting of the winding mandrel, the inner tube, and the two manifold flanges, was removed from the transformer and installed on the winding stand.

The secondary conductor specified in the design requirements stage of the program was to be a cryogenic grade, fully annealed copper foil, 0.01 mm thick and 10 cm wide, and approximately 170 m long. Cryogenic grade was a special order with a one year delivery and a minimum mass of 225 kg. Because of the delivery and mass problem, the requirement was lowered to copper C101,

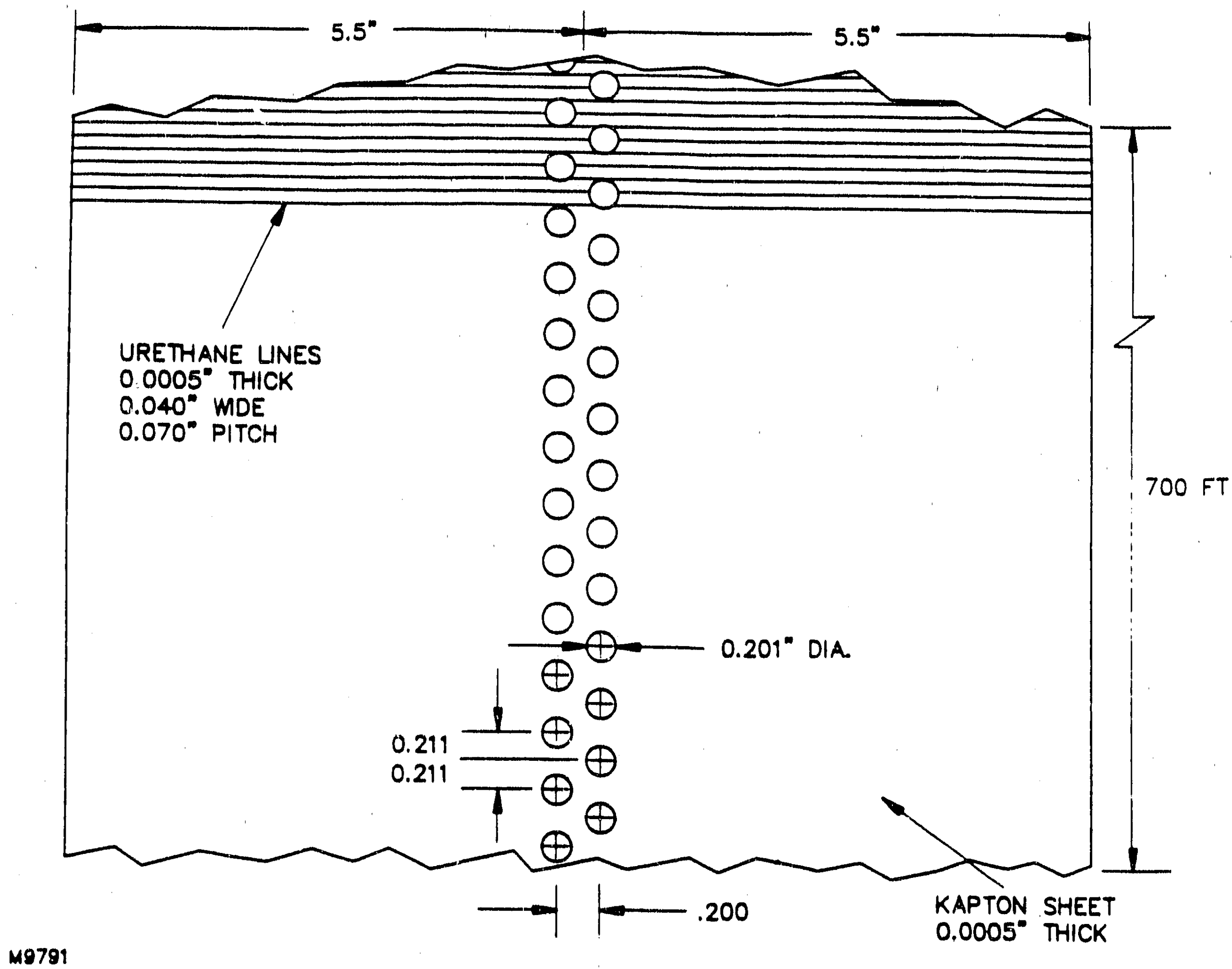

Figure 9 Schematic of the Perforations in the KAPTON Insulating Sheet

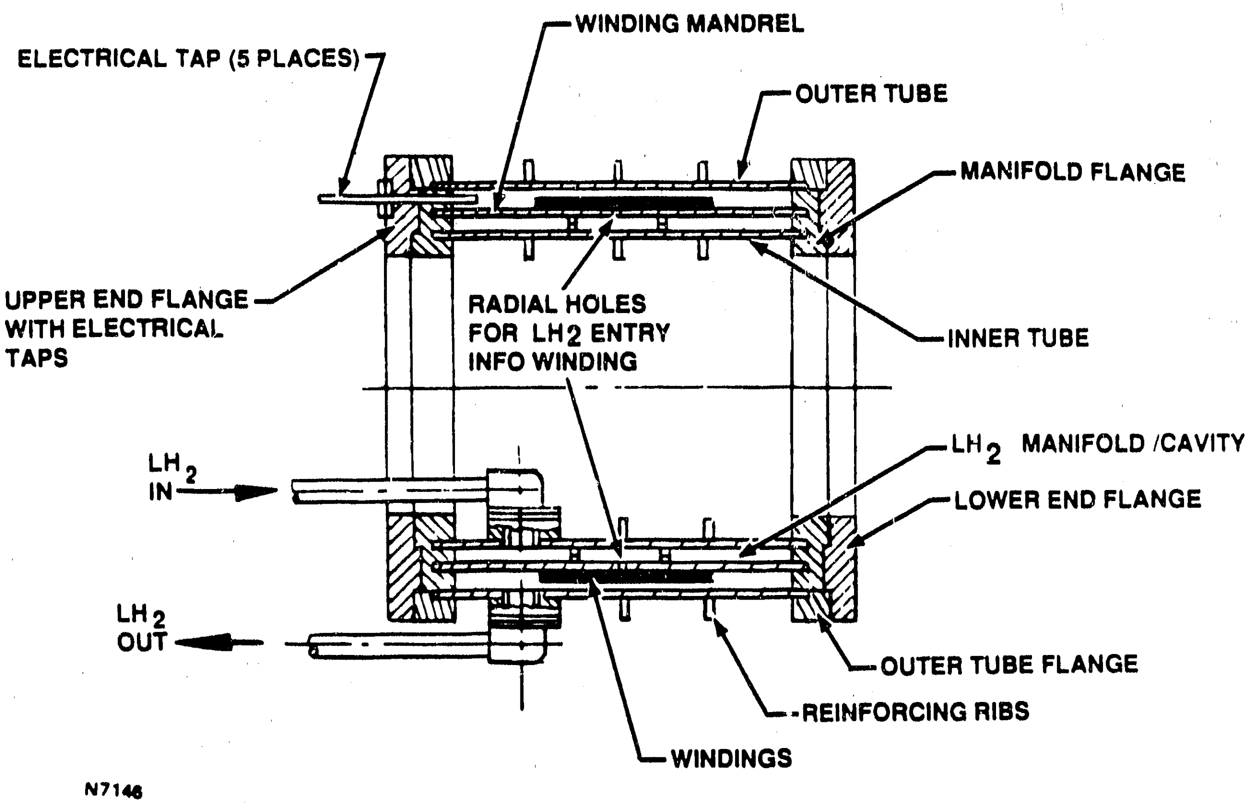

Figure 10 Schematic of the Transformer Construction

which has a higher impurity content and hence higher resistivity by up to a factor of ten than the cryogenic grade. Furthermore, the supplier, AMEX would not anneal the copper foil because the quality of the process control was not sufficient for this very thin material. Lack of annealing results in further decrease in electrical conductivity up to 50 percent. All of these issues were unknown during the detailed design stage of the program because initial contacts with AMEX during the proposal preparation had indicated that they could supply the material in the specified form. Additional problems arose when the vendor supplied the secondary conductor in an insufficient continuous length; the secondary had to be spliced. The net result of all these factors was that the secondary conductor had about five times higher resistivity than the designed assumed. This higher resistivity had to be compensated for by increased coolant flow. Also, the increased resistivity was likely to be the major cause of overheating and insulation failure during the high power testing.

The winding was started by winding three turns of the perforated KAPTON insulating sheet onto the mandrel. The perforations in the KAPTON were aligned with the LH_2 radial holes in the winding mandrel. The secondary conductor, consisting of two, 10 cm wide copper foil strips was started next. Each secondary foil, 0.01 mm thick, was folded out at a right angle to form the electrical leadouts. A continuously speed-adjustable dc motor was used to turn the winding mandrel via a friction drive arrangement. The friction drive and tension spools on the winding stand ensured the proper tension in both the insulator and the conductor. Figure 11 shows the winding of the secondary copper strips.

The winding speed was a fraction of an rpm. The total number of secondary turns is approximately 115. Despite ordering a minimum of 185 m of continuous copper foil, the manufacturer supplied the foils with breaks in them. This caused a significant difficulty. Because the breaks occurred two times on each strip at different points, the tension on the winding had to be released four times. Each time a soldered splice was made, the winding was backed up and rewound to retain the original tension. The schematic of the solder joint is shown in Figure 12. The conductors were overlapped by 23 cm, the solder was placed in the middle, and both were clamped between steel plates. The entire fixture was then heated. (Several test solder joints were

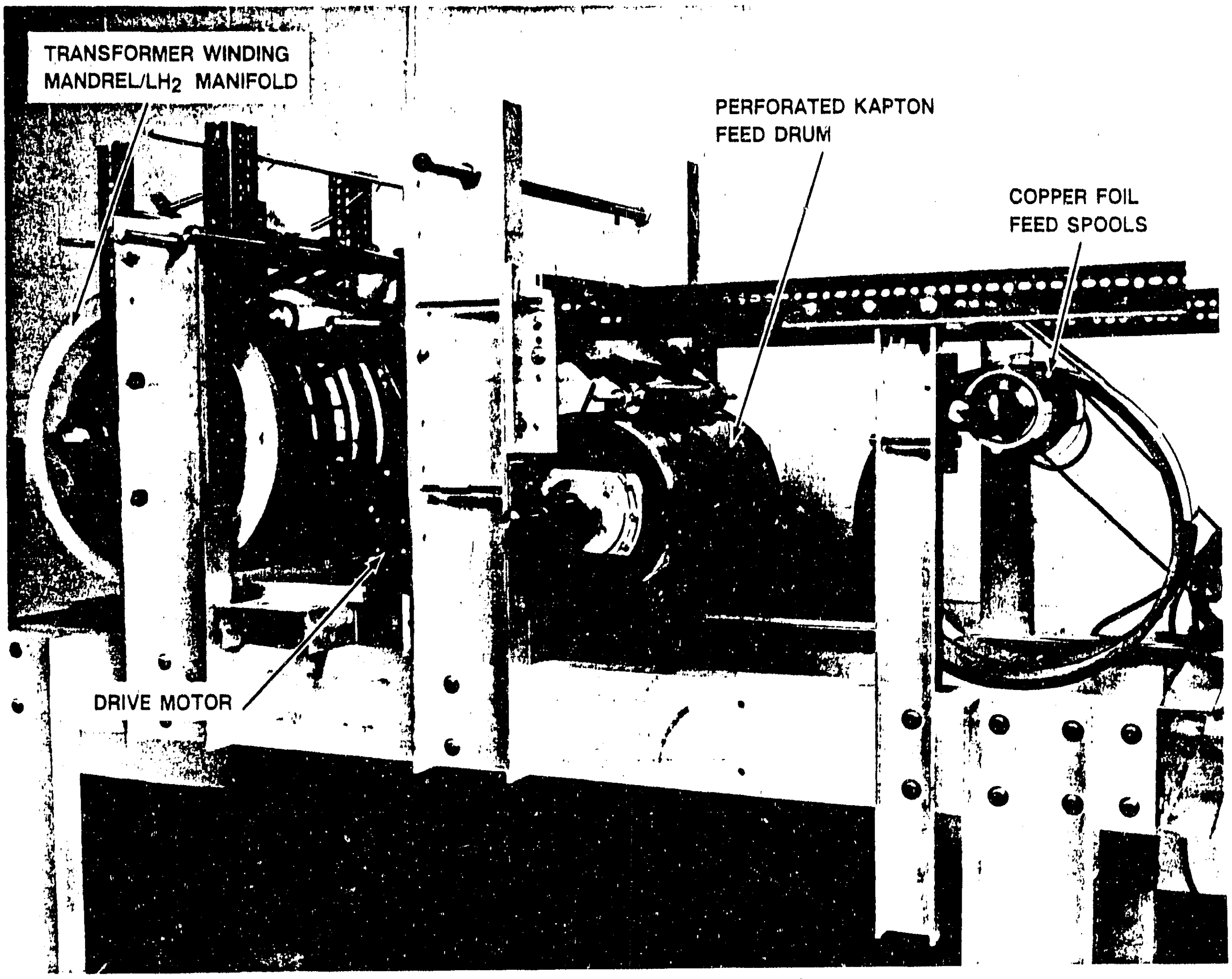

N6647 Figure 11 Photo of Winding in Progress

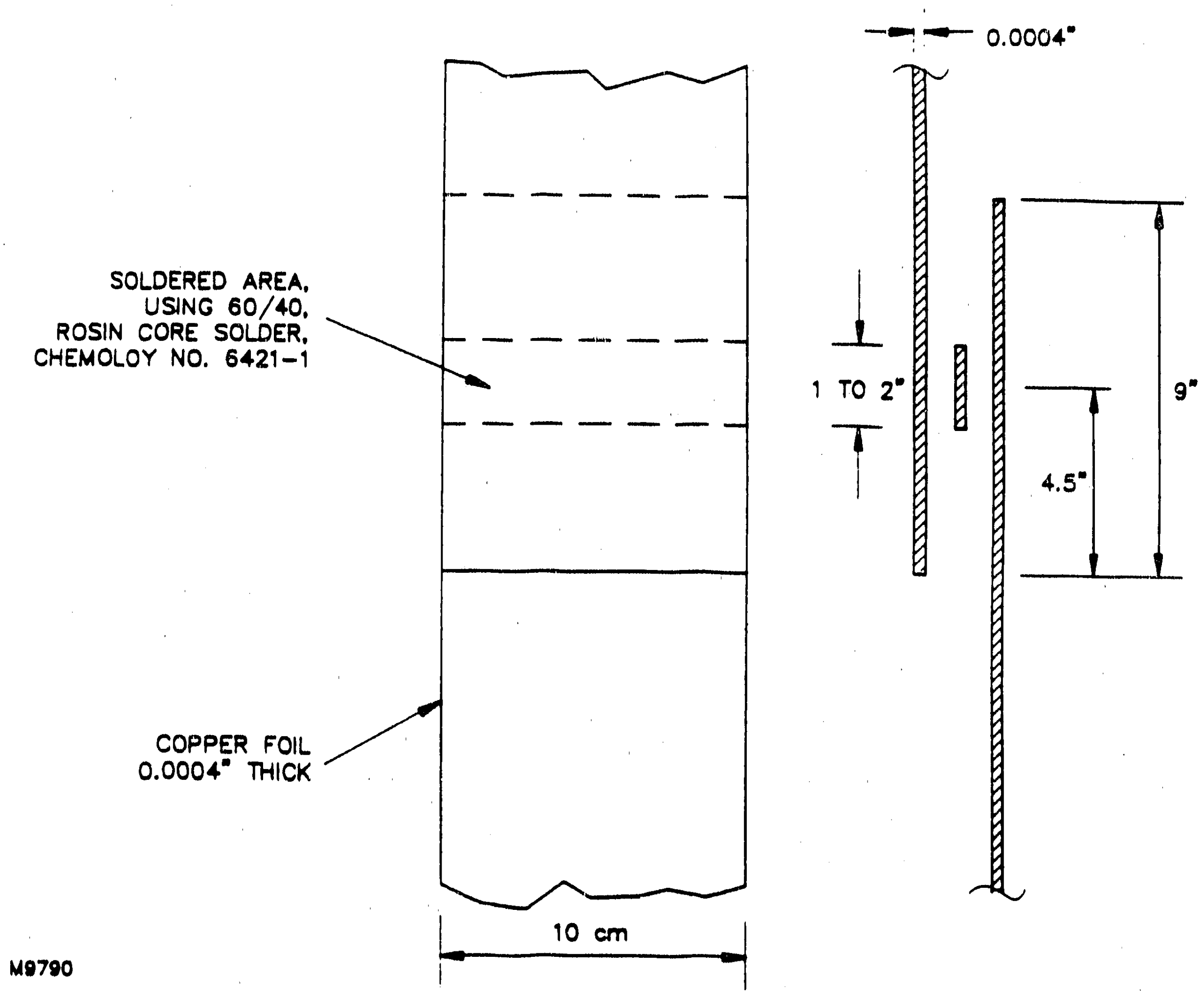

Figure 12 Schematic of the Secondary Coil Splices

made to develop the process.) The strength and electrical conductivity of similar splices at cryogenic temperature was measured previously and was recommended for use in superconducting magnets.[7] Researching the splicing method, developing the fixture, and soldering and rewinding after each break was terminated by a 90° foldout strip for a leadout. The perforated KAPTON was continued for another three turns to band the secondary and to mutually insulate the primary from the secondary.

The primary conductor is 0.089 mm thick annealed copper coil foil. The winding consists of two strips of the same width as the secondary (~10 cm) and was placed directly over the secondary. The total number of the primary turns is 22.4. The mid-tap is located at the midpoint of the primary winding. The fractional turns were necessary to obtain good separation of the terminals, which are schematically shown in Figure 13. The leadouts were formed in the same manner as on the secondary, i.e., each strip was folded out at the start, mid-tap and endpoint of the primary. The winding was banded by five turns of 30 cm wide KAPTON, which was not perforated and does not have the urethane lines. The successive turns were glued to each other by urethane. This band contains the hoop stresses generated in the coil during operation.

Following completion of the winding, the whole transformer was assembled. For cryogenic testing, the transformer was placed in a nonmetallic dewar so that the presence of metal does not influence the magnetic flux distribution of this pure air core transformer. Rather than manufacturing the dewar, an old fiberglass tube section, originally used in conjunction with the Avco 60 cm diameter shock tube that was used to drive a magnetohydrodynamic disk generator, was adapted for the purpose. The tube is approximately 215 cm long and is not a close match to the transformer requirements, but it substantially reduced the cost of the program. The tube was mounted vertically and the transformer was suspended inside it. A vacuum pump and associated connections as well as all electrical feeds were assembled.

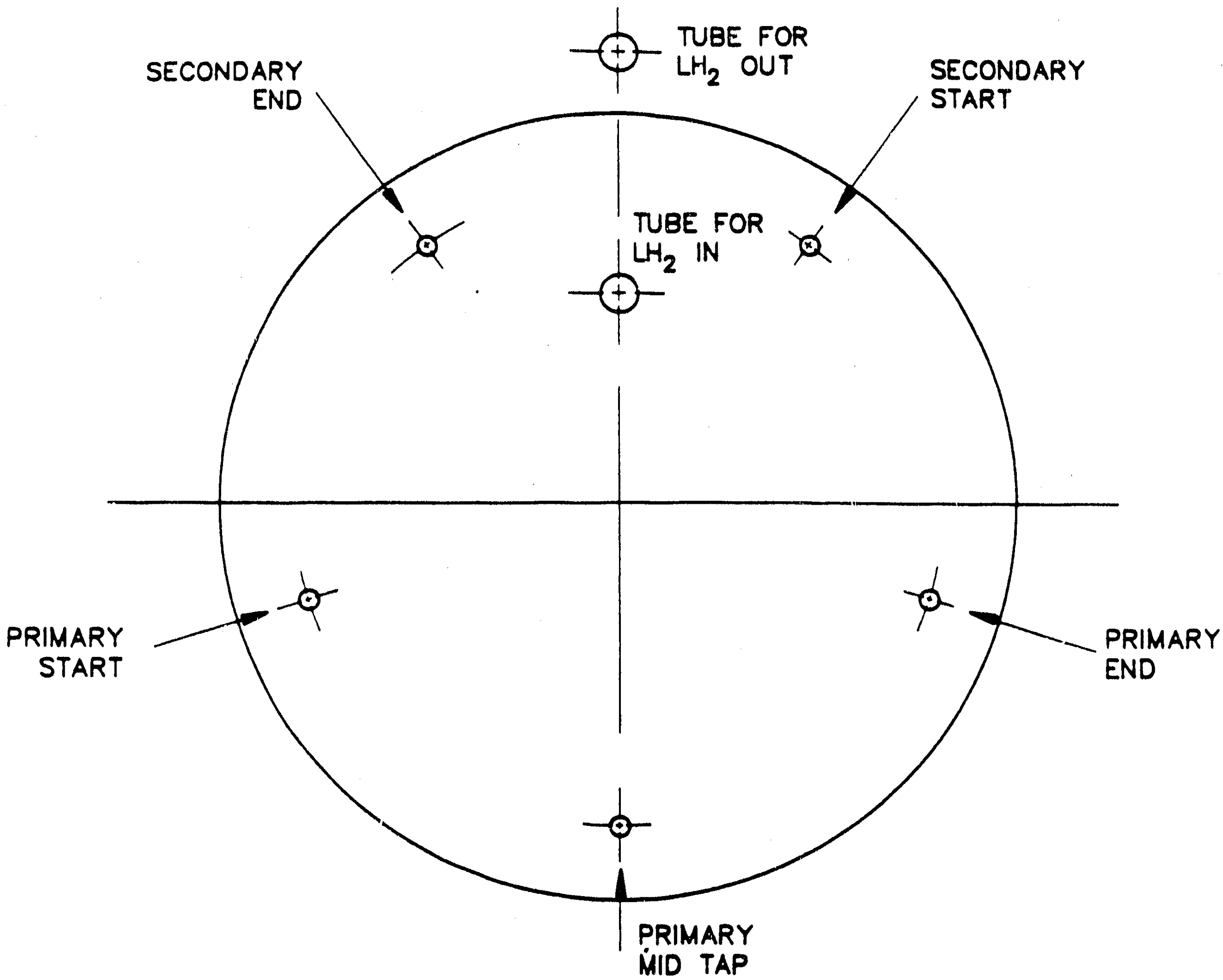

M9789

Figure 13 Schematic of the Start/Termination of the Primary and Secondary Conductors as Viewed from the Top of the Transformer

5.0 LOW POWER TESTING

Three experiments were performed during the low power testing task of the program. First, a set of dummy coils was wound and the coil inductance was measured to determine the accuracy of the predictive formula used in the design of the lightweight transformer. Second, low power tests of the transformer were completed. Testing was conducted at room and liquid nitrogen (LN_2) temperatures. The test variables at each temperature were: a) wave shape - square and sine wave using two different power sources; b) excitation frequency - 100 Hz to 10 kHz; and c) transformer load - Resistance, R_L, from zero to infinity. Third, following low power testing, the transformer was disassembled for inspection. One of the secondary winding foils was partially torn at the terminal. To repair this tear, the primary coil was unwound, and the torn secondary foil was spliced by using the same soft solder joint used during the initial winding. After following the secondary foil repair, the primary coil was wound again over the secondary, and the transformer was reassembled.

5.1 EXPERIMENTS WITH DUMMY COILS

The initial measurements of the self inductance of the transformer coils indicated about 35 percent lower inductance than predicted. A hand held LCR digital meter operating at 1 kHz was used to measure the inductances. In order to determine the cause of this discrepancy, the predictive formula in Equation (14) which was used to calculate the inductance was examined.

$$L = \frac{\mu_o \pi r^2 N^2}{r+b} \qquad (14)$$

where L = self inductance
μ = magnetic permeability
r = winding radius
N = number of turns
b = winding width

There was some uncertainty about the accuracy of this equation because the transformer is wound with two parallel strips with a gap between them, which the formula does not account for. In order to verify this formula, several coils were wound on the existing winding machine from leftover materials from the transformer-KAPTON insulating sheet and secondary winding copper foil. Three types of coils were wound on two PVC pipes with different diameters. The results of these tests are summarized in Figures 14 and 15. In all of the cases, the predicted and the measured values were within 10 percent of each other, which proved that the accuracy of equation (14) for the inductance calculation was acceptable.

All of the inductance data presented in Figures 14 and 15 were obtained using a hand held "Beckman" LCR meter, which operates at 1 kHz. In order to examine the inductance at different frequencies, a power amplifier driven by a sine wave variable frequency generator was connected to the inner coil of the second winding as shown in Figure 15. This coil had 68 turns with its leads folded out in the same manner as the secondary coil in the actual transformer. The input current and voltage were used to calculate the inductance according to the standard equation for L.

$$L = \sqrt{\frac{V_o^2/I_o - R^2}{2\pi f}} \qquad (15)$$

The results are plotted in Figure 16. At frequencies of 500 Hz and higher, the inductance remains essentially constant. This can be contrasted with measurements of the secondary coil in the actual transformer where the measured inductance decreases with increasing frequency.

5.2 LOW POWER TRANSFORMER TESTS AT ROOM TEMPERATURE

The low power testing was conducted at room and liquid nitrogen temperatures. Two different power sources were used. The first was a power amplifier fed by a signal generator (Figure 17) and the second was a dc power supply whose output was switched at 1 kHz with a modified current control circuit, as shown in Figure 18. The power amplifier setup was used to

	NO. OF TURNS N	$R_{PREDICTED}$ (Ω)	$R_{MEASURED}$ (Ω)	$L_{PREDICTED}$ (μH)	$L_{MEASURED}$ (μH)
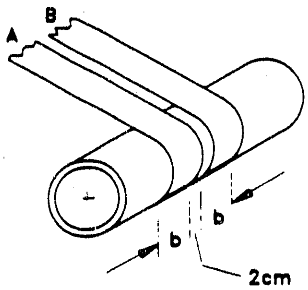 OD = 21.43 cm TWO PARALLEL STRIPS TO SIMULATE THE TRANSFORMER	STRIP A OR B ONLY				
	19	0.214	0.223	78.9	68
	TWO COUPLED STRIPS				
	19	0.107	0.122	49.98	50
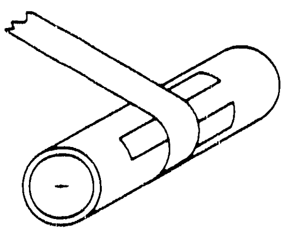 OD = 21.43 cm TWO SEPARATE COILS WOUND OVER EACH OTHER TO SIMULATE PRIMARY & SECONDARY WINDINGS	INNER COIL				
	68	0.799	0.780	999.8	1030
	OUTER COIL				
	10	0.1176	0.130	21.6	23.1

N7976

Figure 14 Summary of Test Coil Measured and Predicted Resistance and Inductance

CONFIGURATION	NO. OF TURNS N	$R_{PREDICTED}$ (Ω)	$R_{MEASURED}$ (Ω)	$L_{PREDICTED}$ (μH)	$L_{MEASURED}$ (μH)
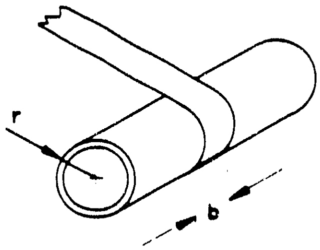 OD TUBE = 12.1 cm FOIL WIDTH = 9.9 cm FOIL THICKNESS = 0.01 mm FOIL MATERIAL = Cu 101 INSULATOR MATERIAL = KAPTON INSULATOR WIDTH = 30 cm INSULATOR THICKNESS = 0.013 mm	15	0.095	0.097	20.1	21.8
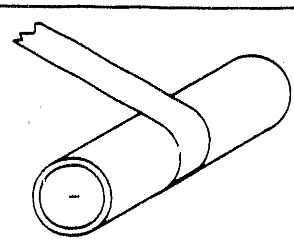 OD TUBE = 21.43 cm NOTE: AFTER APPROXIMATELY 65 TURNS, THE FOIL ENDED, WAS SPLICED WITH ANOTHER FOIL AND THE WINDING CONTINUED TO 130 TURNS. THIS SIMULATES SPLICING IN THE TRANSFORMER	10	0.1176	0.132	21.62	23.0
	20	0.2235	0.241	86.492	90.9
	30	0.33528	0.362	194.61	205
	40	0.447	0.481	345.97	361
	50	0.5588	0.595	540.58	560
	60	0.6706	0.710	778.43	805
	SEE NOTE				
	70	0.782	0.792	1059	1092
	80	0.8941	0.910	1384	1421
	90	1.0058	1.041	1751	1796
	100	1.1176	1.159	2162	2220
	110	1.2936	1.288	2614	2690
	120	1.4112	1.408	3114	3190
	132	1.5523	1.556	3768	3860
	END OF SECOND FOIL				

N7975

Figure 15 Summary of Test Coil Measured and Predicted Resistance and Inductance

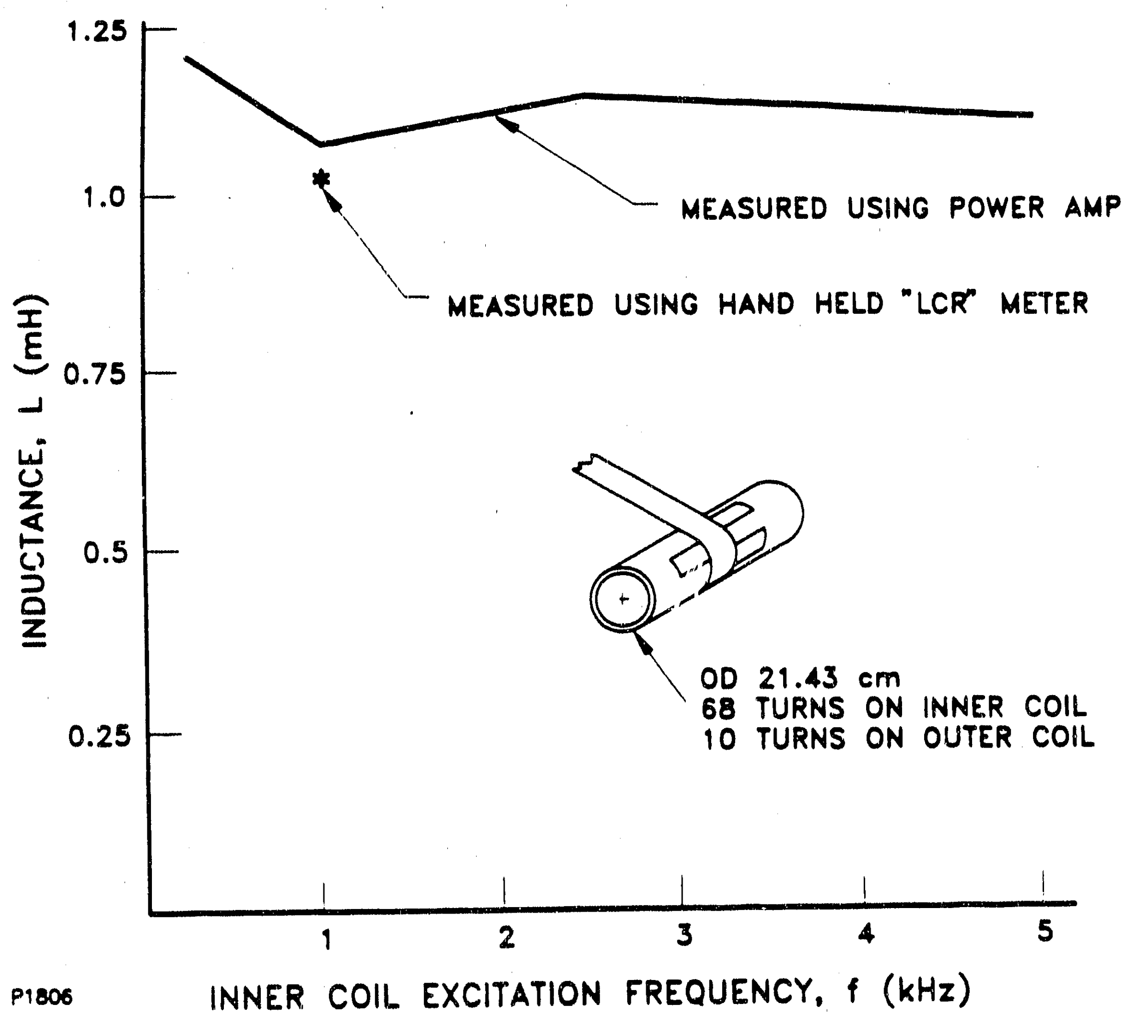

Figure 16 Measured Coil Inductance for Various Excitation Frequencies

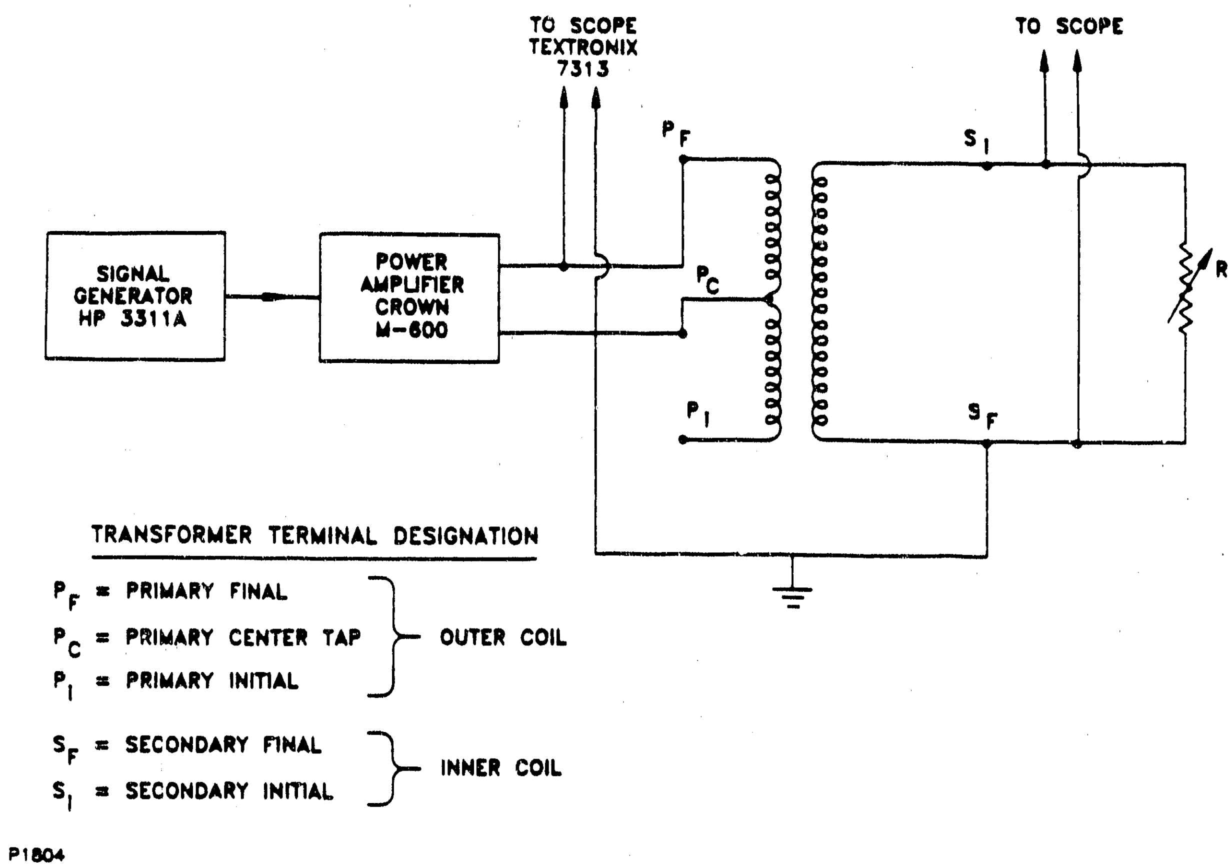

Figure 17 Schematic of the Transformer Test Circuit Using the Power Amplifier and Signal Generator

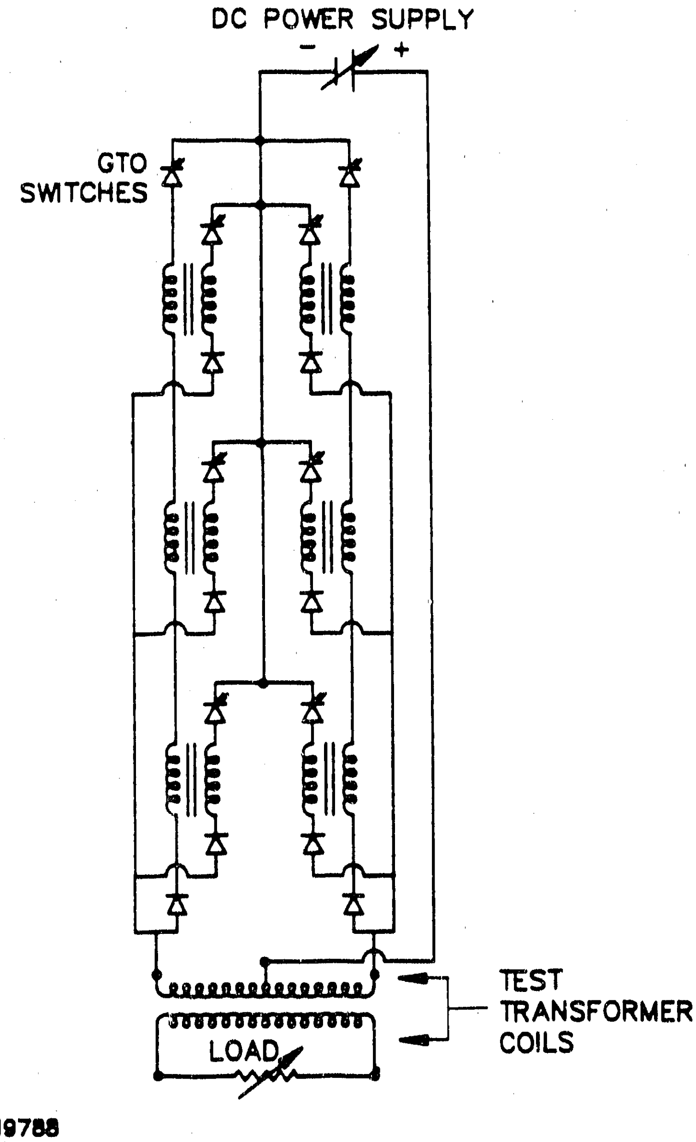

Figure 18 Schematic of the Low Power Transformer Test Circuit

determine the transformer response to a variable excitation frequency under open circuit conditions (infinite load on transformer secondary). The amplifier setup was also used to determine the inductances of the coils. The switched dc supply, shown in Figure 18, was used for tests with the loaded secondary at 1 kHz excitation frequency.

Table 2 shows the values of the inductances and dc resistances of the primary and secondary coils. The measurements were obtained with the power amplifier setup and a digital milliohmeter. The self and leakage inductances were deduced from measured values using Equation (15).

The mutual inductance was calculated using the equation

$$M = \sqrt{\left(L_p - L_p'\right)L_s} \tag{16}$$

The value was checked using

$$M = \sqrt{\left(L_s - L_s'\right)L_p} \tag{17}$$

where the subscripts s and p stand for secondary and primary coils and the L' is the respective leakage inductance. The coupling coefficient k is then given by

$$k = \frac{M}{\sqrt{L_s L_p}} \tag{18}$$

Table 2 shows that the self inductances of the primary and the secondary coils are lower than predicted. The secondary self inductance is 38 percent lower than predicted while the primary self inductance is 28 percent lower than predicted. The build up in the thickness of the winding is responsible for the difference in the leakage inductances, which are directly proportional to the winding thickness. The design thickness of the winding at LH_2 temperature was 6.9 mm, and the measured thickness at room temperature was 11.9 mm. The winding was made "loose" to accommodate contraction of the winding at LH_2 temperature. Further increase in leakage inductance can be explained by the separation of the two strips of conductors that form the

TABLE 2

MEASURED AND DESIGN VALUES OF INDUCTANCES AND WINDING RESISTANCES AT ROOM TEMPERATURE

Measured Values at 1 kHz	Primary (P_C to P_I) ≈ (P_C to P_f)	Secondary S_I to S_F
DC Resistance (ohms)	0.035*	1.43*
Self Inductance (μH)	42.6	3740
Leakage Inductane (μH)	9.9	850
Mutual Inductance (μH)	350.8	--
Coupling Coefficient (-)	0.88	--
Design Values at 1 kHz		
DC Resistance (ohms)	0.015	1.36
Self Inductance (μH	59.2	6000
Leakage Inductance (μH)	2.65**	264

*Includes resistance of terminal connections
**At LH_2 temperature with contracted windings

windings. The contraction of the winding was expected to result in a decrease in the winding thickness, and hence, the leakage inductance.

The lower self inductances of both the primary and the secondary are more difficult to explain, especially because the driving coil measurements agreed with the prediction within 10 percent. In order to understand this, the coils were excited at various frequencies to determine if conductor ac resistance or large interwinding capacitance was lowering the apparent self inductances. The results of the secondary coil variable frequency measurements are plotted in Figure 19. Corresponding results for the primary winding are shown in Figure 20 (center tap to end of winding).

At 100 Hz, the measured self inductance, L, corresponds to the design value and drops with increasing frequency, f. The dummy coils discussed in the previous section had self inductance nearly independent of frequency (Figure 16). Therefore, the transformer may have interwinding and leadout parasitic capacitance that distorts the measurements. In order to confirm this, the coil was modeled as shown in Figure 21. The equations for the effective inductance, L_e, and resistance, R_e, were used to calculate the effective impedance, Z_e, which was matched to the measured $Z = V_0/I_0$. The capacitance was varied parametrically from 1 μF to 1 nF, but a good match between the measured Z and calculated Z_e was not obtained.

Thus, neither analysis nor supporting experiments with dummy coils successfully explained the discrepancies between the measured and predicted values of the inductances and the frequency dependence of the self inductance of the coils. This topic is discussed in more detail in Section 6. Nevertheless, the transformer operated quite satisfactorily as indicated in subsequent discussion.

Typical oscilloscope traces of the primary (center tap to end) and the output secondary voltages under no load conditions are shown in Figure 22. The schematic of the test circuit is shown in Figure 17. The oscilloscope photos are arranged in descending order of excitation frequency, starting at 2.5 kHz, 1 kHz and 250 Hz.

The design value of the secondary to primary voltage ratio was ten. This compares well to the experimental value of 9.6 obtained at or below 1 kHz. At frequencies of 2 kHz and above, this ratio dropped to about nine.

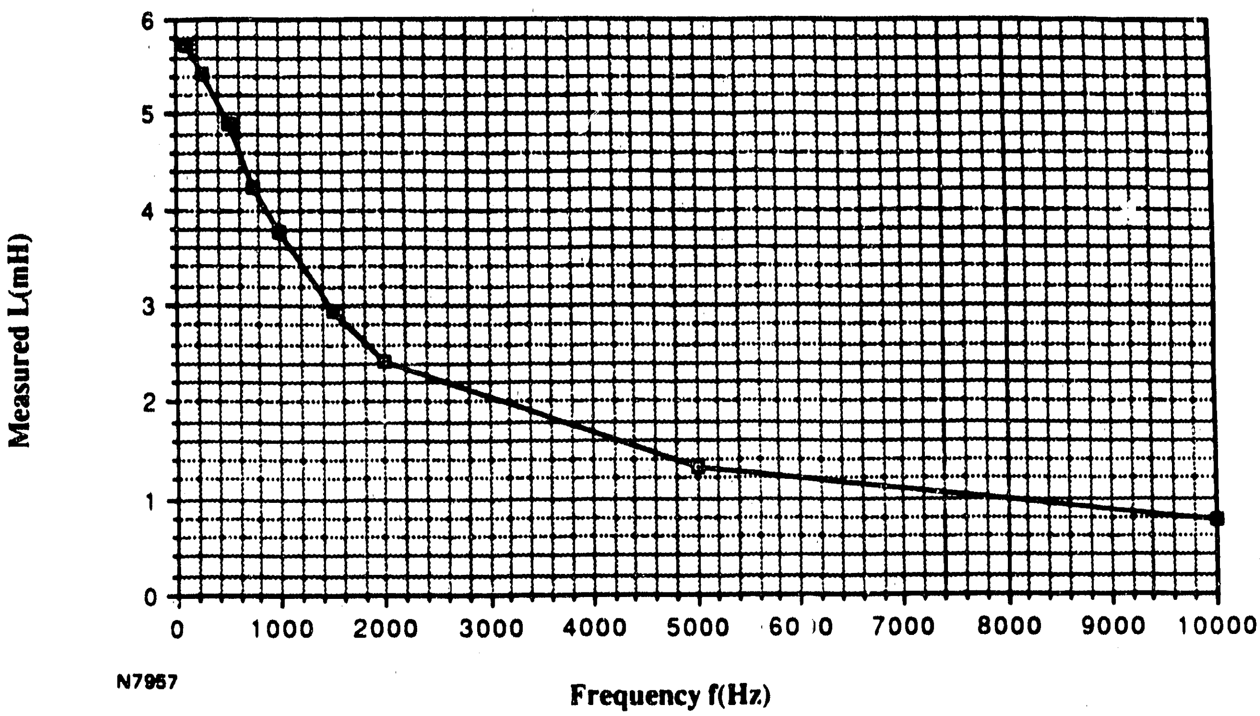

Figure 19 Self Inductance of the Secondary Coil As a Function of the Excitation Frequency

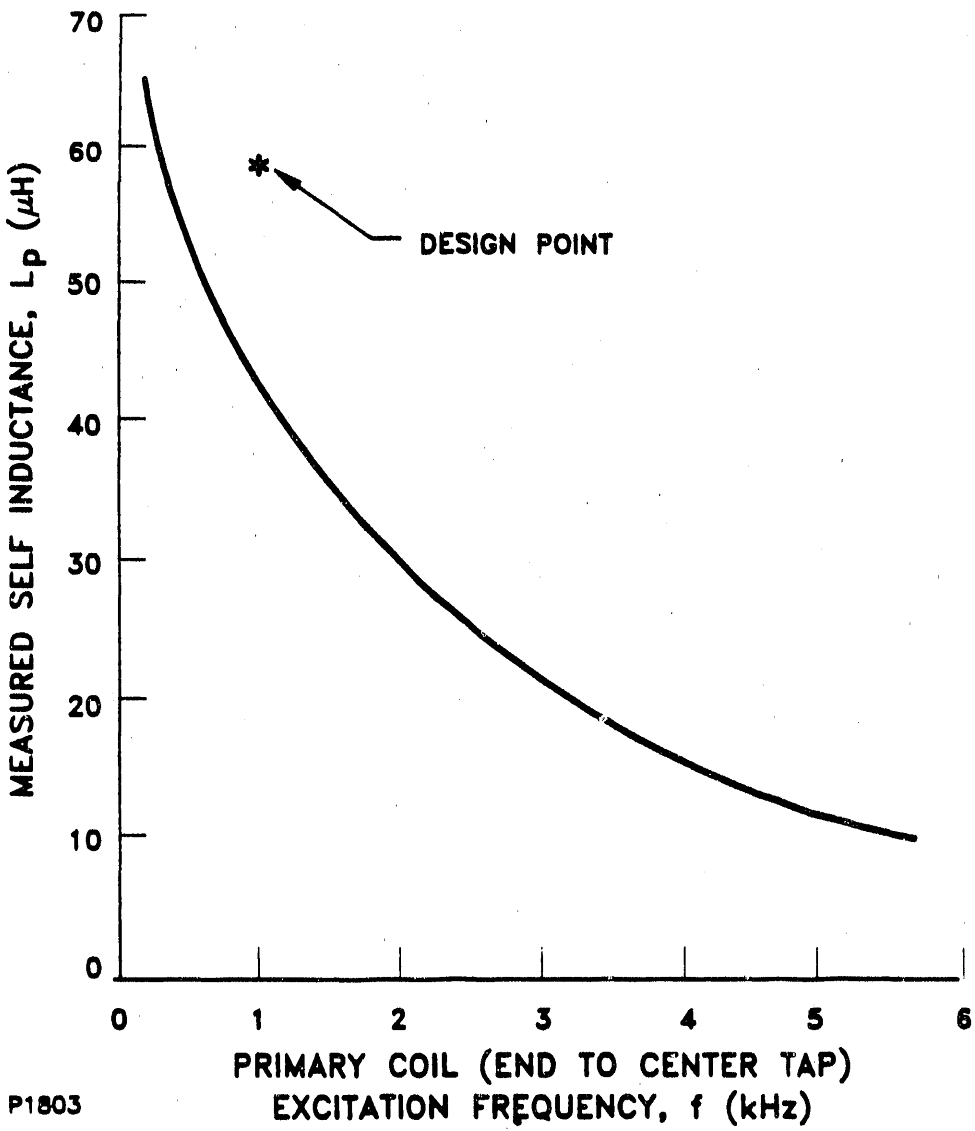

P1803

Figure 20 Measured Self Inductance for Various Excitation Frequencies

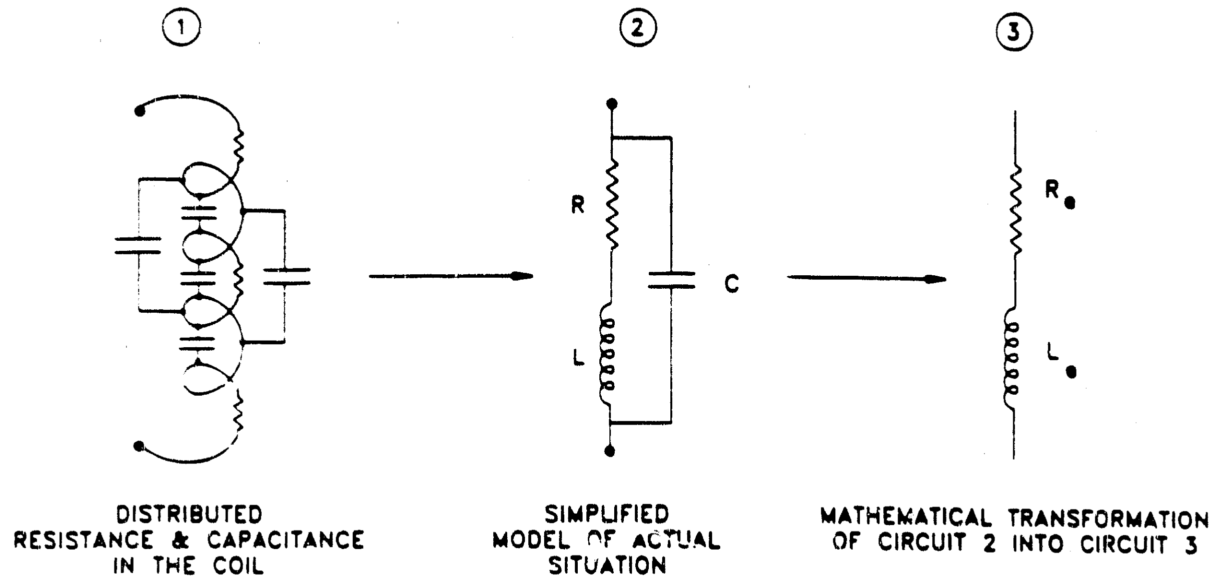

$$L_e = \frac{L(1-\omega^2 CL) - CR^2}{\omega^2 C^2 R^2 + (\omega^2 CL - 1)^2}$$

$$R_e = \frac{R}{\omega^2 C^2 R^2 + (\omega^2 CL - 1)^2}$$

WHERE R = IS AN AC RESISTANCE OF THE SAME LENGTH STRAIGHT WIRE TO ACCOUNT FOR SKIN EFFECT

P1805

Figure 21 Schematic of Modeling of the Actual Coil

DATA FROM 5/3/89
USING POWER AMP ON P_F TO P_C

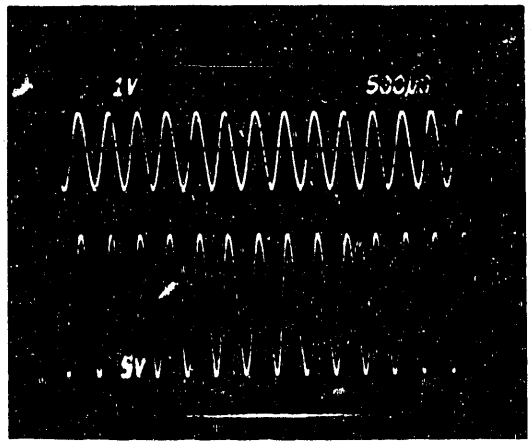

f = 2.5 kHz, $R_L = \infty$

PRIMARY VOLTAGE

$$\frac{V_S}{V_P} = 9.1$$

SECONDARY VOLTAGE

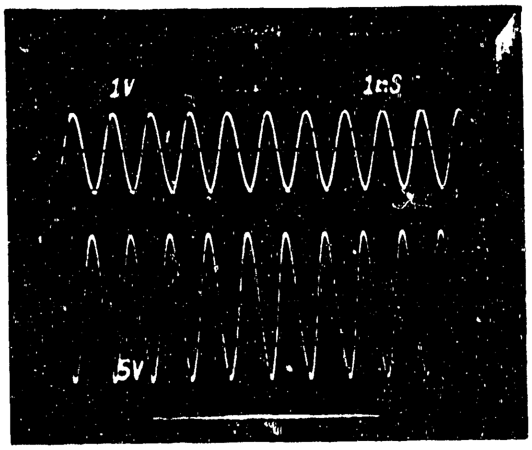

f = 1 kHz, $R_L = \infty$

PRIMARY VOLTAGE

$$\frac{V_S}{V_P} = 9.6$$

SECONDARY VOLTAGE

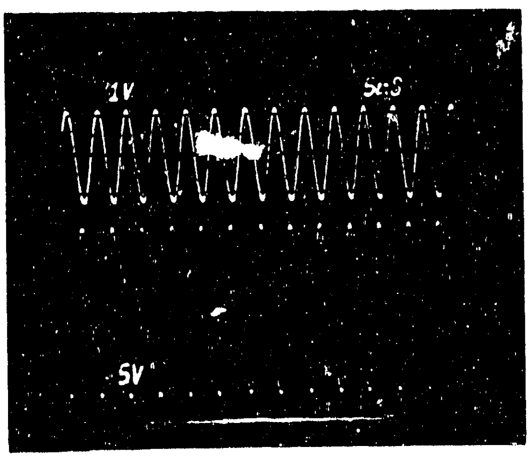

f = 250 Hz, $R_L = \infty$

PRIMARY VOLTAGE

$$\frac{V_S}{V_P} = 9.6$$

SECONDARY VOLTAGE

N7980

Figure 22 Typical Primary and Secondary Voltage Traces at Various Frequencies

Tests at frequencies from 10 kHz to 100 Hz were conducted with using both sine and square waves. At 100 Hz, both the sine wave and the square wave became distorted. The transformer was unable to support the imposed voltage. The distortion was less evident when the other half of the primary winding was used and disappeared above 150 Hz. Thus, the transformer clearly can operate over a broad range of frequencies.

A typical example of oscilloscope traces with a loaded secondary of $R_L = 50\ \Omega$ and with a square wave input to the primary is shown in Figure 23. The top photo shows the primary voltage and current while the bottom shows the corresponding traces of the secondary. The frequency was 1 kHz. The figure shows that the secondary voltage and current droop is minimal.

After tests that used one-half of the primary fed by a power amplifier (Figure 17), tests were performed using a dc power supply switched by the modified current control circuits (Figure 18). This circuit is a small scale version of the one to be used during the high power test. Because of the existence of this circuit that allows the switching of hundreds of amperes at 1 kHz, the transformer was designed with a center tapped primary. In this configuration, the transformer was tested with a range of loads from open circuited to short circuited secondary. The switching frequency with this circuit is fixed at 1 kHz. A typical example of the waveforms obtained with $R_L = 2.5\ \Omega$ and $R_L = 0$ is shown in Figures 24 and 25, respectively. The primary voltage and current are shown on the top photos and the secondary voltage and current are shown on the bottom. With loads above 10 Ω, the secondary to primary voltage ratio (V_s/V_p) was nearly equal to the design value of 10. At loads below that resistance, the room temperature secondary coil resistance of ~1.4 Ω becomes comparable to the load; hence, the voltage regulation of the transformer is affected. Thus, the V_s/V_p ratio at $R_L = 2.5\ \Omega$ dropped to 5.9. At LH_2 temperature, the 2.5 Ω is the design load. Because the coil resistance drops at cryogenic temperature, the voltage regulation of the transformer is unaffected.

DATA FROM 5/8/89

USING POWER AMP ON P_C TO P_i

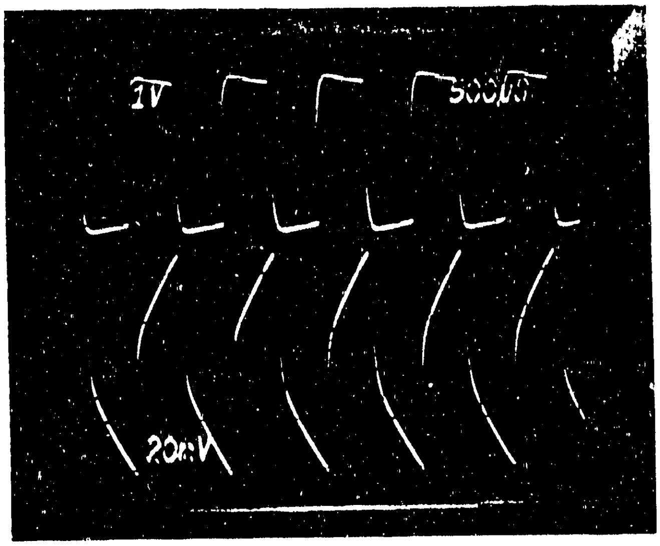

f = 1 kHz, R_L = 50 Ω

PRIMARY VOLTAGE
1V/division

PRIMARY CURRENT
5A/division

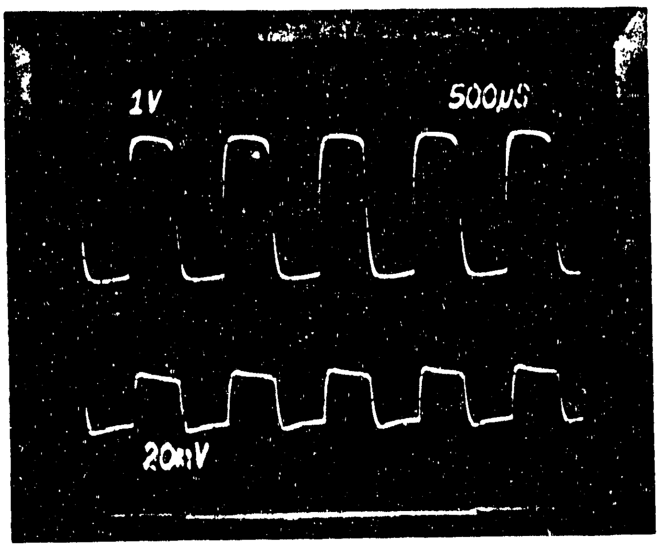

SECONDARY VOLTAGE
10V/division

SECONDARY CURRENT
0.5A/division

N7979

Figure 23 Typical Oscilloscope Traces of Primary and Secondary Voltage and Current Measurements with 50 Ω Load

DATA FROM 5/6/89
USING DC SUPPLY & CC CIRCUIT

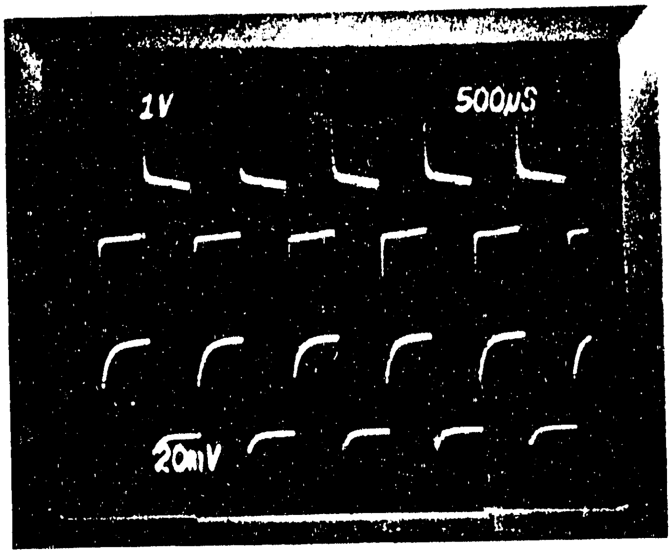

f = 1 kHz, R_L = 2.5 Ω

PRIMARY VOLTAGE (P_C TO P_i)
1V/division

PRIMARY CURRENT (INTO P_i)
5A/division

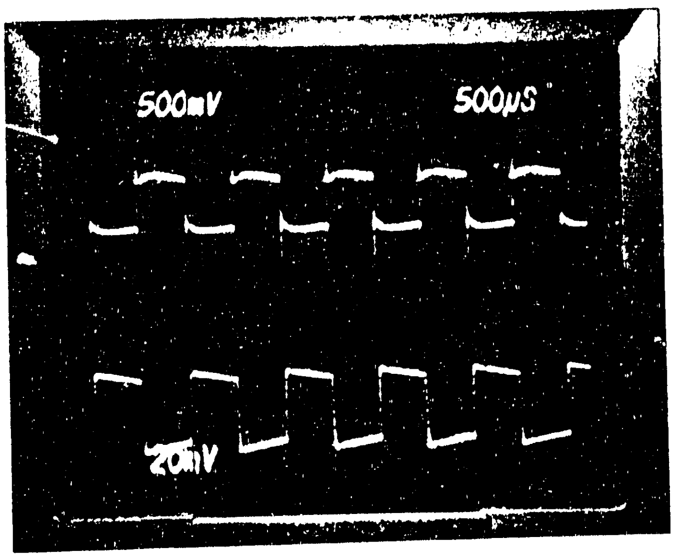

SECONDARY VOLTAGE
5V/division

SECONDARY CURRENT
1A/division

N7978

Figure 24 Typical Waveforms of the Primary and Secondary Voltages and Currents at R_L = 2.5 Ω

DATA FROM 5/6/89
USING DC SUPPLY & CC CIRCUIT

f = 1 kHz, R_L = 0

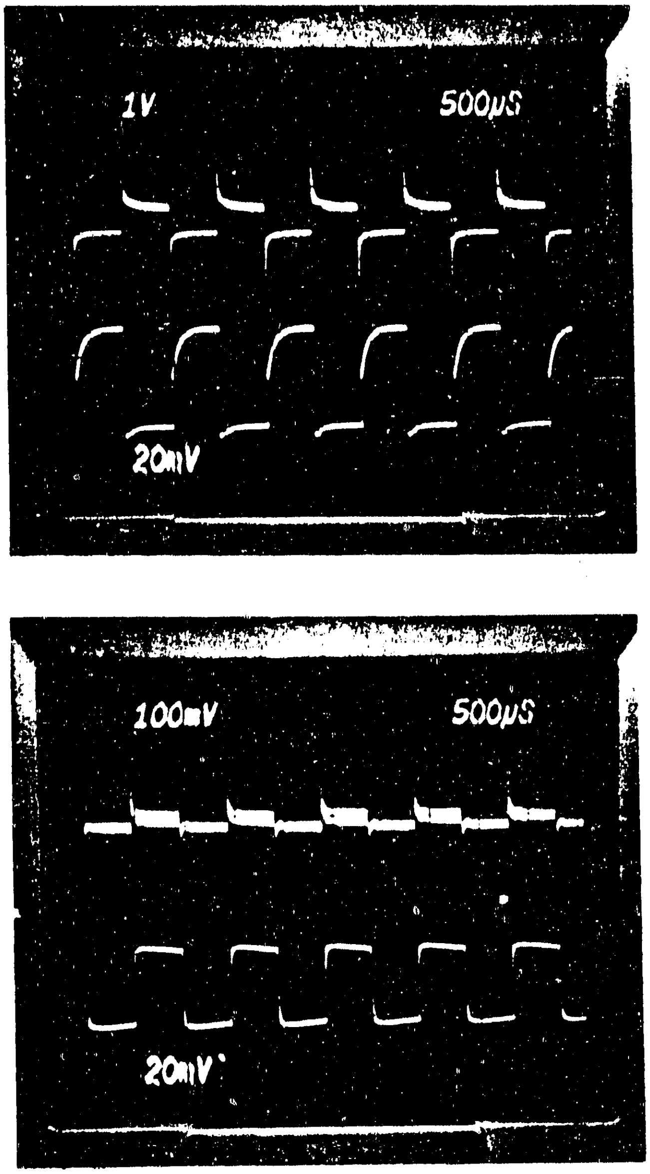

PRIMARY VOLTAGE P_C TO P_i)
1V/division

PRIMARY CURRENT (INTO P_i)
5A/division

SECONDARY VOLTAGE
1V/division

SECONDARY CURRENT
1A/division

N7977

Figure 25 Typical Waveforms of Primary and Secondary Voltages and Currents at R_L = 0 (Short Circuited Secondary)

5.3 LOW POWER LN_2 TESTING TRANSFORMER AT LN_2 TERMPERATURE

After the room temperature tests, the transformer was inserted into a container that was evacuated to minimize heat leaks to the transformer. An old, existing fiberglass tube 60 cm in diameter and approximately 2.5 m long with strong end flanges was adapted for the purpose. This tube was an inexpensive alternative to making a new, geometrically more convenient dewar out of non-magnetic materials. To minimize heat leaks, the transformer was suspended from the top flange of the 60 cm tube and all cryogen and power lines were brought through this flange via Swagelock bulkhead fittings that were vacuum sealed with urethane. All O-rings exposed to LN_2 were made from polyamide materials that seal at cryogenic temperatures. A mechanical vacuum pump connected to the dewar constantly maintained the vacuum in the dewar. The LN_2 was delivered to the transformer through an insulated line from a conventional cryocylinder.

From a mechanical point of view the areas of greatest concern were: 1) breakage of the copper conductor because of its shrinkage when exposed to the cryogen; and 2) sealing of the cryogen with non-metallic materials. Because of the concern over the potential for breakage of the copper conductor, the electrical continuity of the secondary coil was continuously monitored during the transformer cool down process. The transformer was cooled down to LN_2 temperature (77K) three times and held at the temperature for several hours while handling a maximum primary current of 120 A. After completion of the test series, one leg on the secondary conductor was found partially torn, which was believed to have occurred during assembly/disassembly of the transformer. Other than that, both the primary and the secondary conductors remained intact, thus eliminating the greatest design concern.

During the first cool down/warm up cycle, there was a partial loss of vacuum in the 60 cm diameter tube. This indicated a leak of cryogen from the transformer into the evacuated tube. The transformer was removed and all flange fasteners were retightened with the transformer partially filled with LN_2. As subsequent tests showed, the cryogen gas leak diminished but was not eliminated. The small leak could not be located because it only occurred with the transformer filled with LN_2. When the transformer was removed from the evacuated tube at this temperature, it quickly frosts up. The rapid ice buildup prevented effective leak detection.

From an electrical point of view, the transformer performed well at all loads. However, similar to the room temperature conditions, the unexplained frequency dependence of the inductances persisted.

A value of greatest importance was the ratio of the room temperature to liquid nitrogen temperature conductor resistivity. As reported previously the supplier delivered the secondary conductor as rolled copper not annealed, and also, the conductor was supplied in several sections that required soft solder splicing. Furthermore, the most important difference between the initial design and what was ultimately delivered is that the conductor was made out of Cu 101 instead of Cu 10100, which is a high purity cryogenic grade. This substitution was accepted because the cost difference in the small quantity required was an order of magnitude. All of these changes--unannealed copper, splicing, and lower purity copper--increased the resistivity of the conductor at cryogenic temperature.

The measured ratio of room temperature to LN_2 temperature resistance for the secondary and primary conductors (including stainless steel terminals) is 6.39 and 5.93, respectively. The corresponding secondary coil conductor resistivity is 0.25×10^{-6} Ω-cm, which means that the room temperature resistance ratio, RRR, value defined in Figure 13 is slightly over 20. By using Figure 26 for predicting the resistivity at LH_2 temperature (20 K), a resistance of 7.0×10^{-8} Ω-cm can be expected. The design value was 1.7×10^{-8} Ω-cm, which should have been easily achievable with the original design conductor. This increased resistivity resulted in increased cooling requirements, lower voltage regulation, and lower efficiency than initially predicted. Because of the increased cooling requirements, the high power test time was reduced from the original plan. However, these difficulties are clearly the result of the low quality of the copper conductor provided by the supplier. The measured leakage inductances are given in Table 3.

TABLE 3

Measured Leakage Inductances at Room Temperature and LN_2 Temperature

	Primary Leakage Inductance (μH)	Secondary Leakage Inductance (μH)
Room T	9.9	850
LN_2 T = 77 K	22.3	570

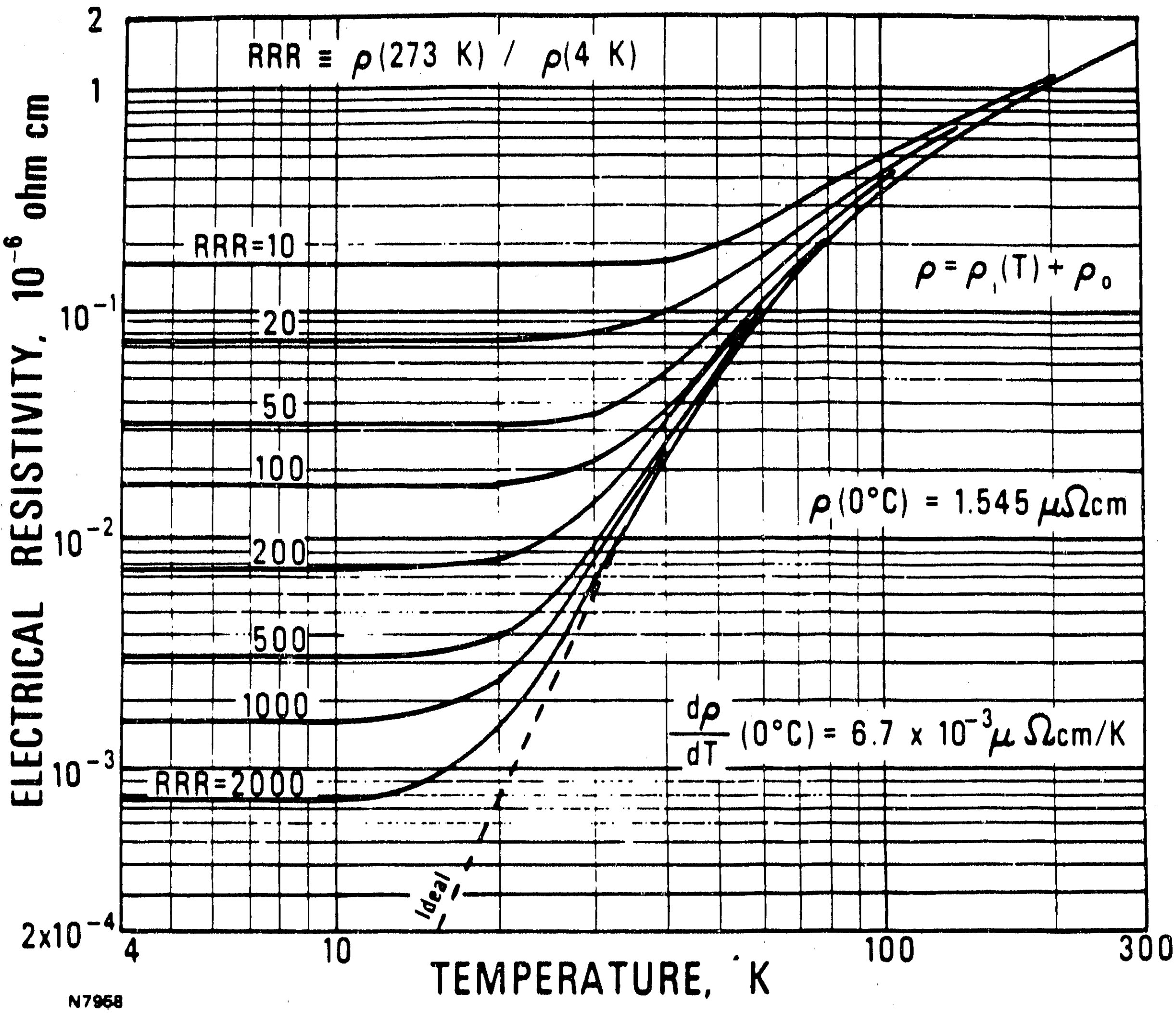

Figure 26 Electrical Resistivity of Copper As a Function of Temperature

As Table 3 shows, the secondary leakage inductance decreased as was anticipated. Leakage inductance is directly proportional to the winding radial thickness. Thus, when the coil contracts, its radial thickness diminishes and the leakage inductance decrease. However, contrary to anticipation, the primary leakage inductance increased. A possible explanation and suggested remedy follows. The primary coil in this transformer is wound over the secondary as is done in room temperature air core transformers. The windings have the same width but the primary foil thickness is ten times greater than the secondary. Thus, the secondary winding is likely to have contracted more than the primary and opened up a radial gap between the two coils. Therefore, the leakage inductance of the primary increased. The obvious solution in future designs is to wind the secondary over the primary so that the secondary contracts onto the primary.

The maximum primary current during this low power testing at LN_2 temperature was 120 A. This limit was imposed by the existing current control switching circuit which consisted of 4 GTO switches in parallel, each switch can handle about 30 A. The maximum voltage imposed on the secondary was 200 V. (One thousand volts is projected for the high power testing.) Typical waveforms with a load of 2.5 Ω are shown in Figure 27. The top photo shows the primary voltage and the secondary current, and the bottom photo shows the corresponding secondary voltage and the same secondary current as in the top photo. The current probe could not handle the 120 A primary current. So, this current is not displayed but was measured with an analog dc ammeter. The voltage regulation improved substantially over the room temperature case at the same load as shown in Figure 24. At room temperature, the secondary to primary voltage ratio (V_s/V_p) was about six. As expected, at LN_2 temperature this ratio increased to eight because of lower coil resistance. The design objective at LH_2 temperature is $V_s/V_p = 10$. As mentioned earlier, the open circuit $V_s/V_p = 9.6$.

The power balance at this load is as follows. The input into the primary was approximately 300 watts and the output to the 2.5 Ω load was approximately 155 watts as is easily computed from traces in Figure 27. Because the transformer has no core, the only losses are I^2R losses. In the primary, these losses were $(120)^2$ (.0059) = 85 watts, and in the secondary they were $(15.5)^2$ (.219) = 53 watts. The sum of delivered power plus I^2R losses is 293 watts, which is reasonably close to the input of 300 watts. The

DATA FROM 5/19/89, LN_2, PHOTO 34 & 35
DC POWER SUPPLY

f = 1 kHz, R_L = 2.5 Ω
PRIMARY CURRENT ON P.S. ≅ 120A

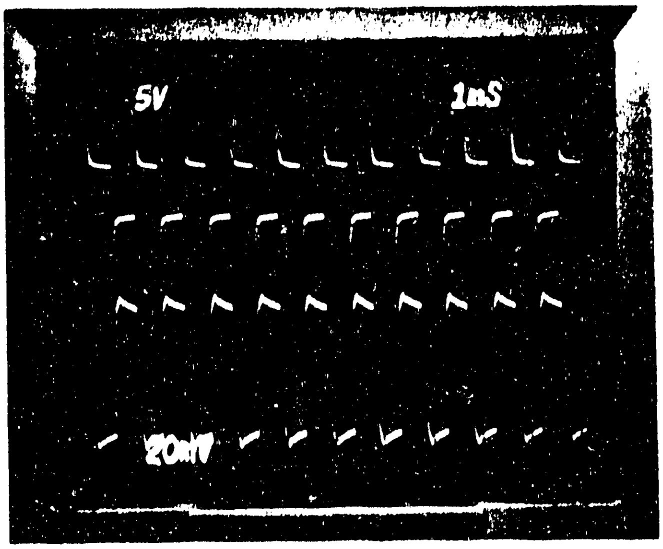

PRIMARY VOLTAGE (P_C TO P_i)
5V/division

SECONDARY CURRENT
5A/division

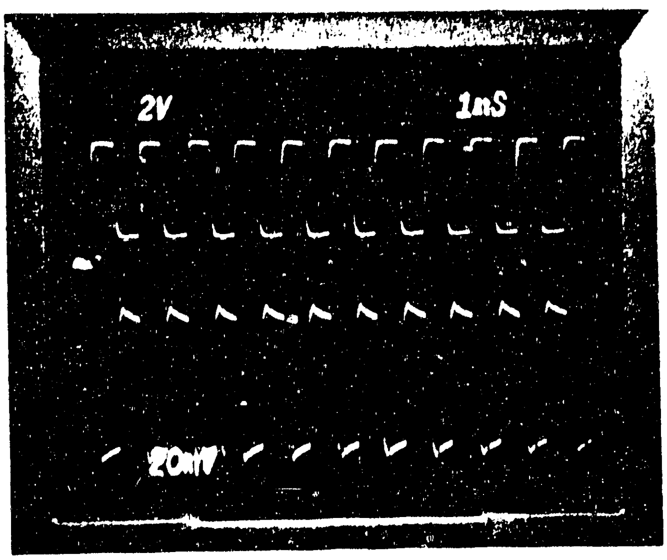

SECONDARY VOLTAGE
20V/division

SECONDARY CURRENT
5A/division

N7981

Figure 27 Typical Waveforms of Primary and Secondary Voltages and Secondary Currents with R_L = 2.5 Ω and Primary Current of 120 A dc difference can be easily accounted for by measurement inaccuracies and possibly by a small loss caused by dielectric losses.

In general, except for the increase in the primary leakage inductance, the transformer performed well at LN_2 temperature.

6.0 HIGH POWER TESTING

The low power tests at room LN_2 temperatures were completed in May 1989. The transformer was disassembled, i.e., the winding was removed from its outer shell and inspected. A small tear was found in one of the secondary coil copper foil leadouts. The damage was likely to have been caused by the previous assembly. To repair the damage, the primary winding was unwound, and the secondary leadout was spliced and reconnected to the terminal. The primary was wound back over the secondary, and the winding was reinstalled in its outer shell. A series of resistance and inductance tests were performed to determine if any changes occurred. None were detected; all measurements, i.e., primary and secondary resistance, self and leakage inductances remained the same as previously reported. The transformer was then shipped to Avco for high power testing.

The power supply, the 1 kHz switching equipment, and the transformer load to be used for the high power testing at Avco are an integral part of the Mk VI/Mk VII magnetohydrodynamic test facilities. The 7 MW electrical power supply is normally used to power the test facility magnets, the switching circuits are used in the magnetohydrodynamic current controls, and the water-cooled load resistor bank is used as the electrical load for the magnetohydrodynamic generator. Because the coal-fired magnetohydrodynamic power system tests were assigned a higher testing priority by DOE, the transformer work proceeded only when these facilities were idle. Thus, most of the transformer setup and testing was performed after hours and on weekends.

The schematic of the initial test circuit is shown in Figure 28. The block diagram of the same circuit is shown in Figure 29. The current control circuits force current equilization/sharing within each group that consists of 15 slaves (inner circuits in Figure 28) and one master (outer circuit). Eight groups are required to switch 4000 A, which was the maximum planned primary current. Current sharing between groups was obtained by small resistors as indicated. Special triggering/gate control circuits were built to ensure synchronization of all GTO's in each phase. Switching was performed at 1 kHz. For initial testing and shakedown of the instrumentation, only two groups of the current control were used. This approach permitted a maximum primary current of approximately 1000 A.

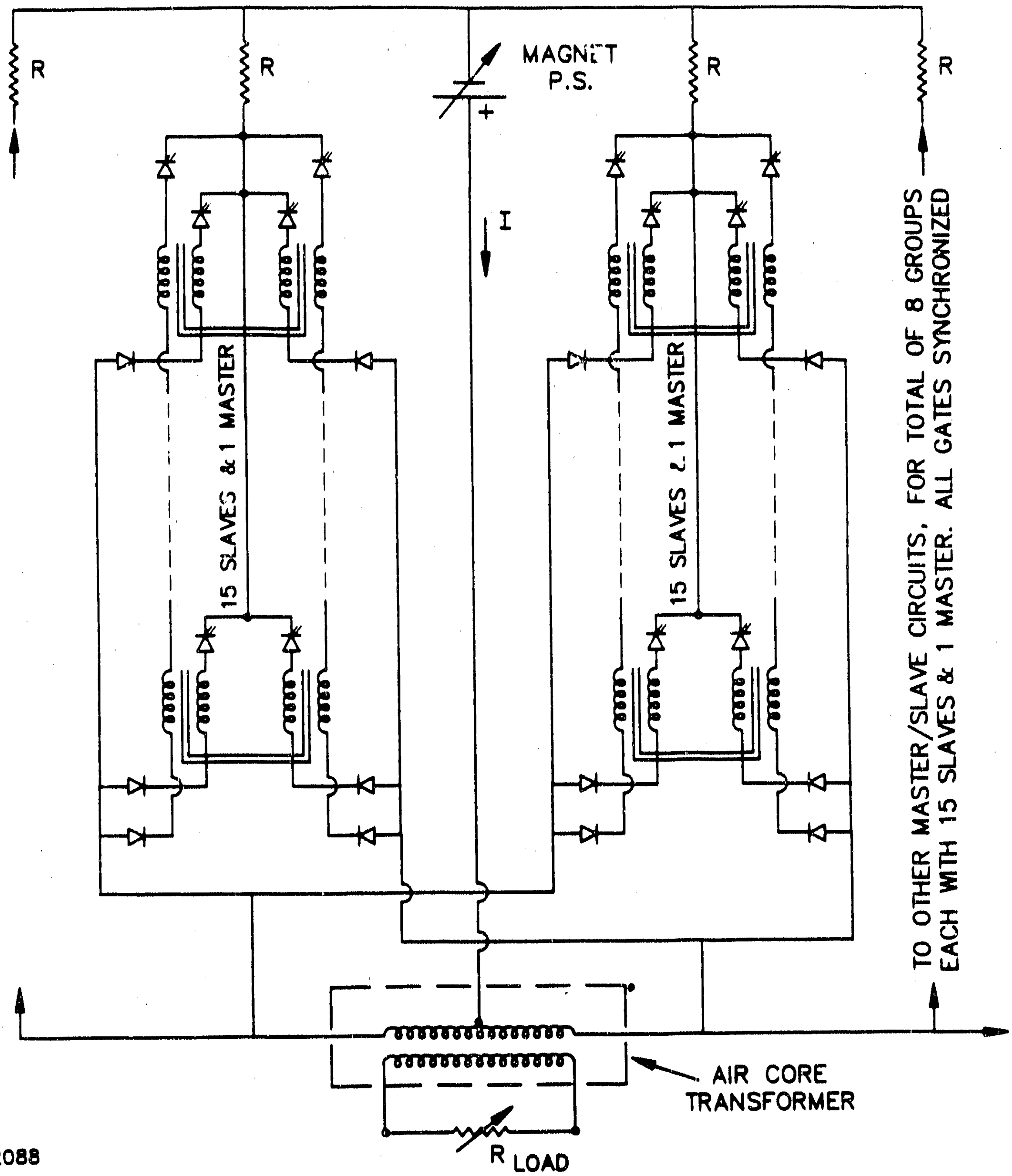

P2088

Figure 28 Schematic of the Initial Test Circuit

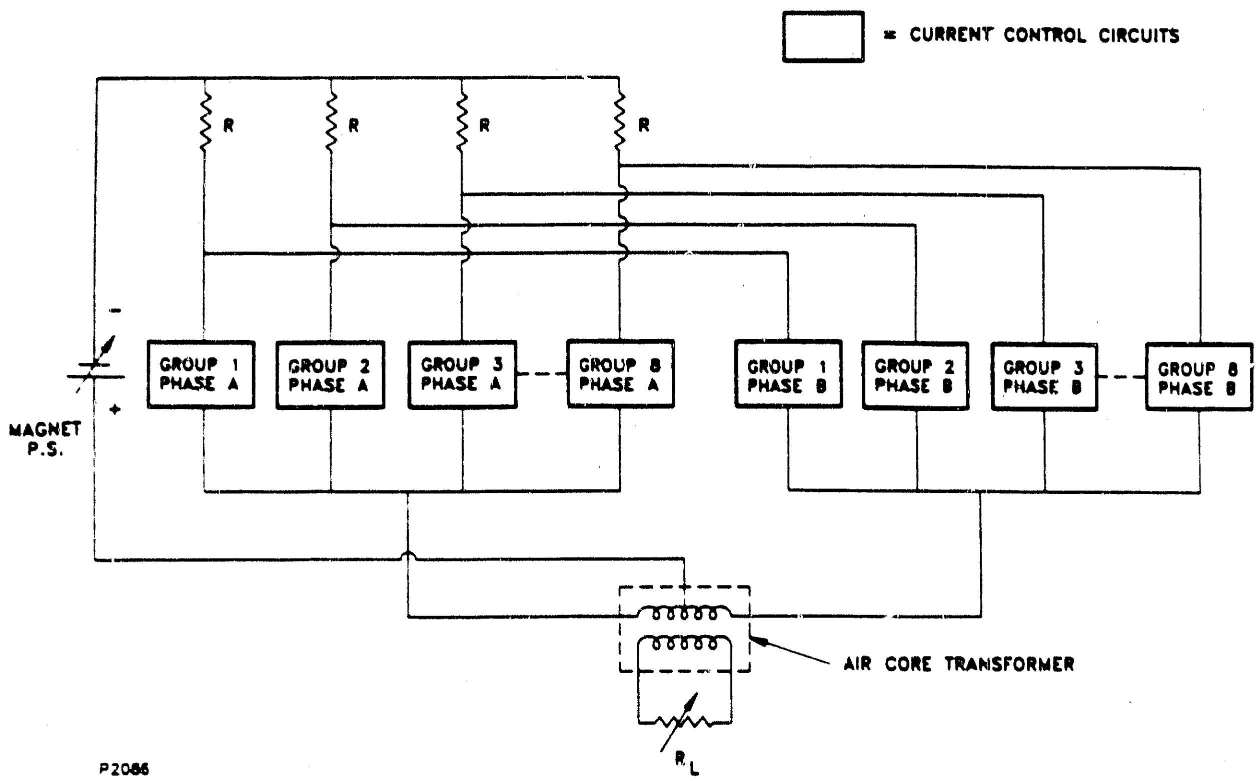

Figure 29 Block Diagram of the Transformer Test Circuit. Up to 4000 A Primary Current Switched By Current Control Circuits (128 GTO's in Parallel for Each Phase).

The first test that used the magnet power supply revealed that the SCR controlled supply was very poorly filtered. At low current, a few hundred amperes, the power supply output current was discontinuous. A typical current waveform from the power supply obtained with a 5 Ω load is shown in Figure 30. The frequency is 360 Hz, which originates in the 6 pole SCR bridge. This waveform is of course an unacceptable input into the transformer so a filter had to be constructed. An LC filter was assembled from available, unused equipment. The inductance was 10.3 mH and the capacitance was 3200 μF. Further tests revealed that the electrical load bank had too large an inductance (a nichrome wire wound on a cylinder submerged in circulating water). Therefore, a rectifier bridge with a capacitive filter was built and connected between the transformer secondary and the aforementioned load. The final schematic of the transformer test circuit is shown in Figure 31. The locations of the current and voltage transducers are indicated.

The newly installed test facility computer was used to record the output of the transducers. Each data channel was sampled at 10 kHz to obtain at least ten points per cycle of the transformer. Because of this fast sampling rate which was not previously tested, many problems were encountered in obtaining reliable data. These problems included high frequency coupling of the transducer outputs, transducer nonlinearity, ground loops, etc. To resolve these problems the transformer was tested both at room temperature and at liquid nitrogen temperature many times. The number of tests at room temperature at typical primary currents up to 100 A was approximately twenty-five. Because of the problems with instrumentation and the efforts to debug the system, some of these tests lasted up to one hour of continuous power transfer. The number of the transformer cool down cycles to LN_2 temperature (including tests carried out at Busek during low power testing) was twelve. Each time, the transformer was held at LN_2 temperature (77 K) for minimum of two hours. Typical test durations with power applied ranged from 30 to 60 sec. The load was varied from 1 Ω to 50 Ω.

After all instrumentation and data recording systems were debugged and ready for testing, an attempt was made to run the transformer at LN_2 temperature with up to 1000 A primary current. This current was estimated to be the limit at LN_2 temperature. The internal power dissipation at 1000 A at LN_2 temperature is approximately equal to that which occurs at the design point of 4000 A at LH_2 temperature. During this test, the transformer

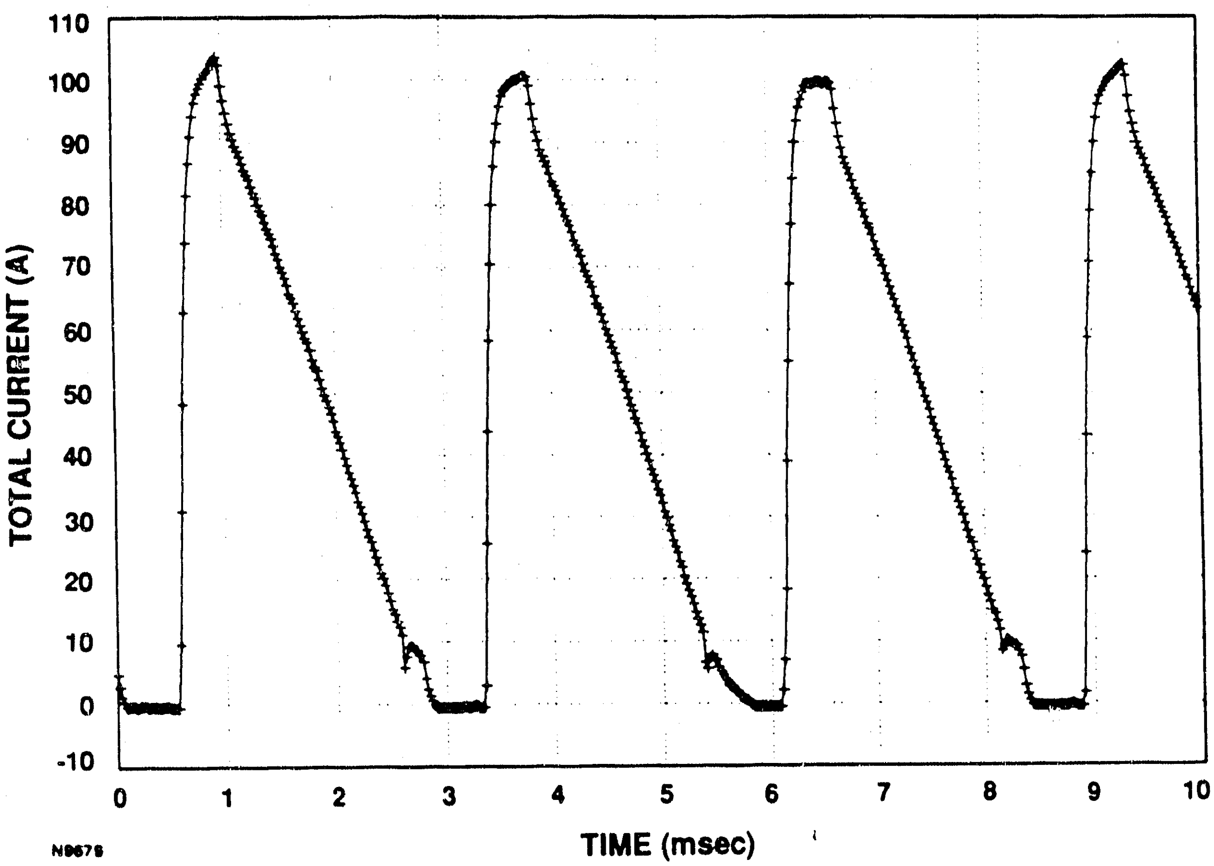

Figure 30 Typical Current Waveform from the Power Supply with a 5 Ω Electrical Load

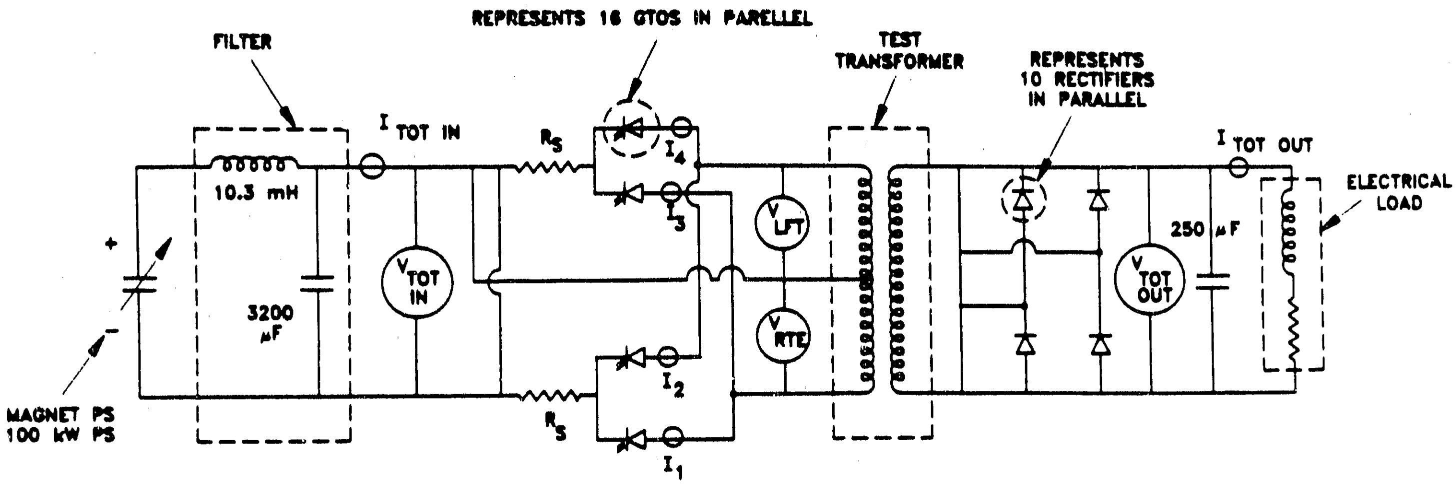

Figure 31 High Power Lightweight Transformer Test Schematic Final Configuration

winding (primary turns and primary to secondary) intermittently shorted. The primary current is shown in Figures 32 and 33. The former shows the current over a 20 sec. period after start and the latter shows the 10 msec period 10 sec. into the test. Although the peak currents revealed in both figures are not believable (caused by transducer overshoot), intermittent shorts with currents reaching several thousand amperes existed. The power supply is capable of delivering 12,000 A. The corresponding rectified output (secondary) currents are shown in Figures 34 and 35. The primary and secondary voltages are shown in Figures 36 and 37, respectively.

The initial damage is believed to have been caused by operating the transformer without coolant at the 100 A level for prolonged periods of time to debug the data acquisition system and test facility. During this period, the transformer insulation apparently overheated which caused several shorts under the highly stressed condition. The failure was reported to DOE and testing was terminated because of lack of funds. The transformer was removed from its dewar and outer shell and inspected. No visually observable damage was detected. Post failure photographs of the winding are shown in Figure 38.

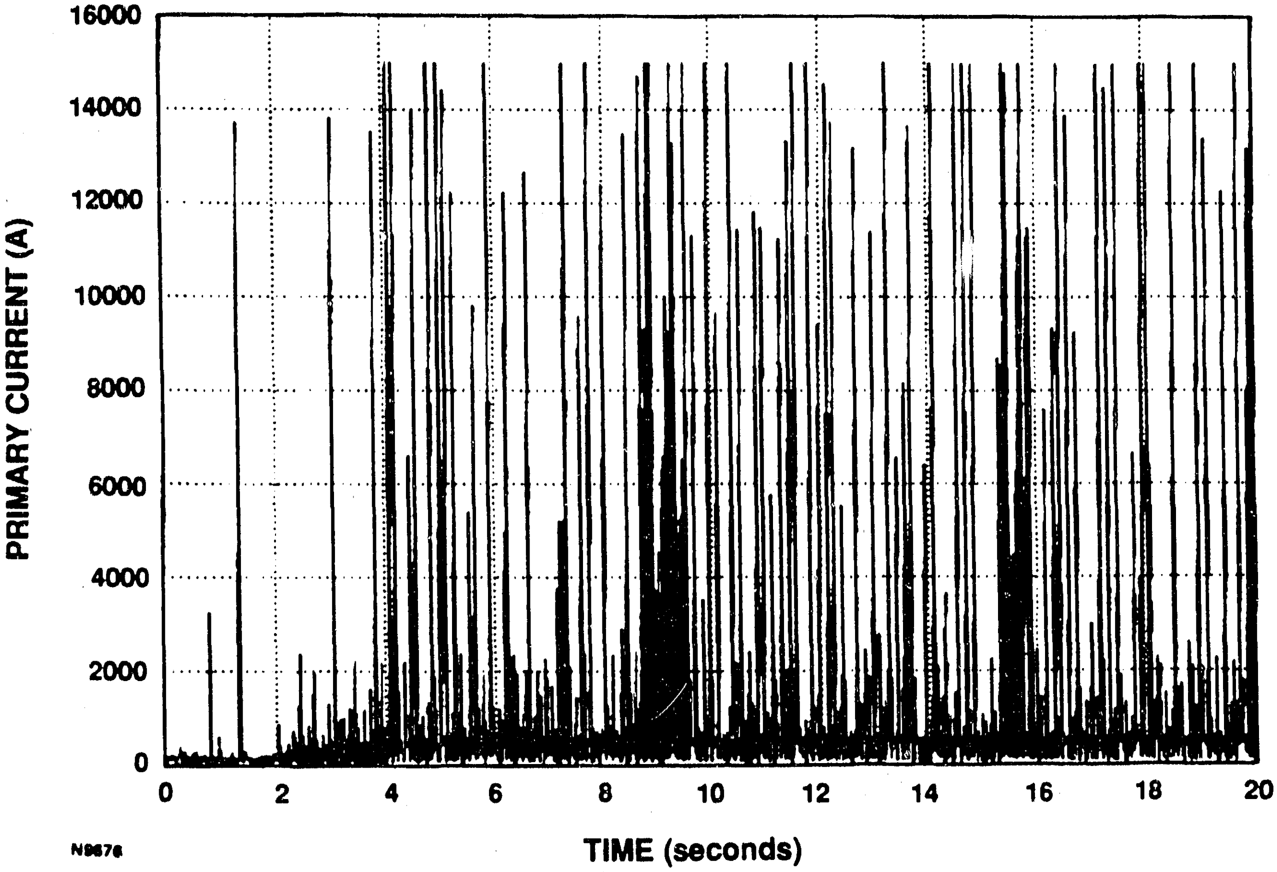

Figure 32 Primary Current Over a 20 sec Period After the Test Start

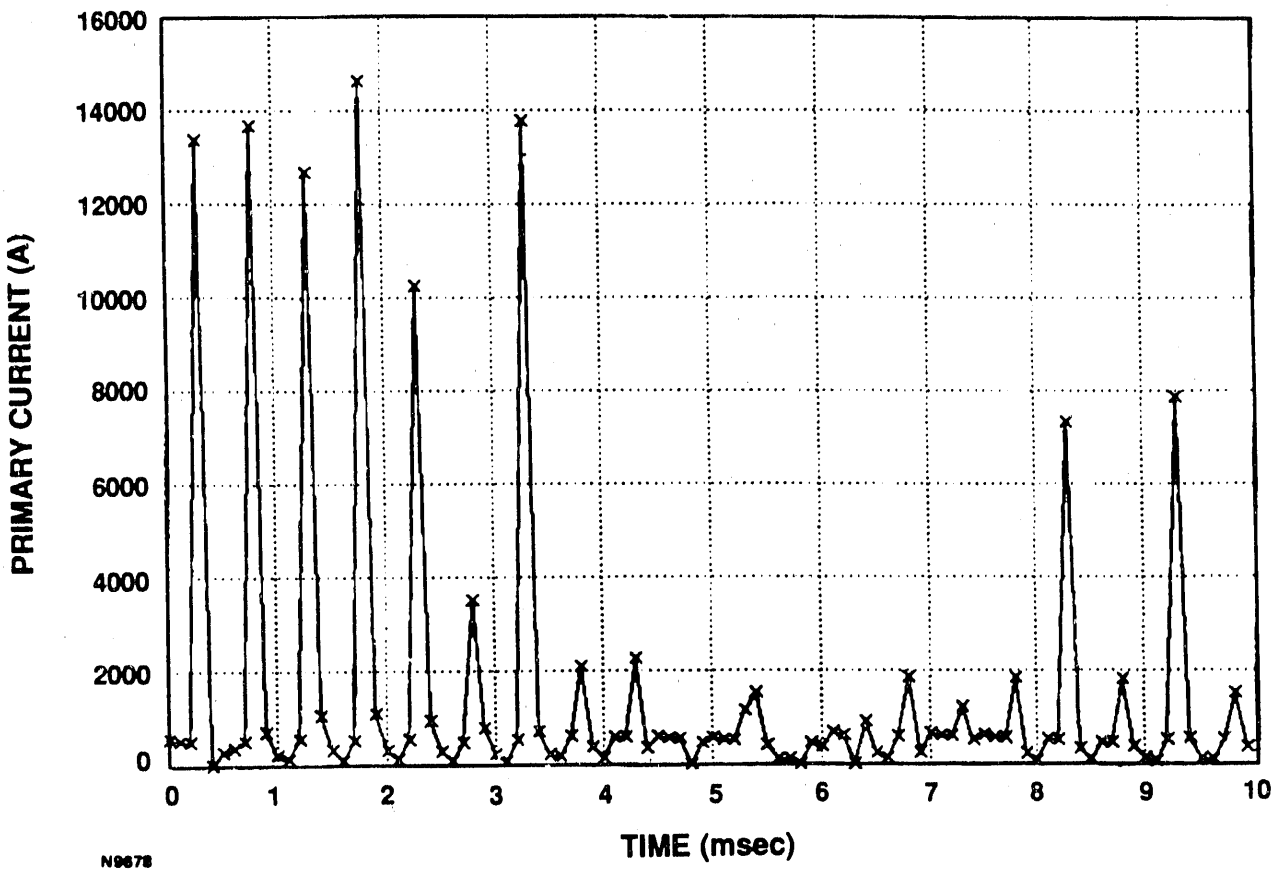

Figure 33 Primary Current Over a 10 msec Period 10 sec into the Test

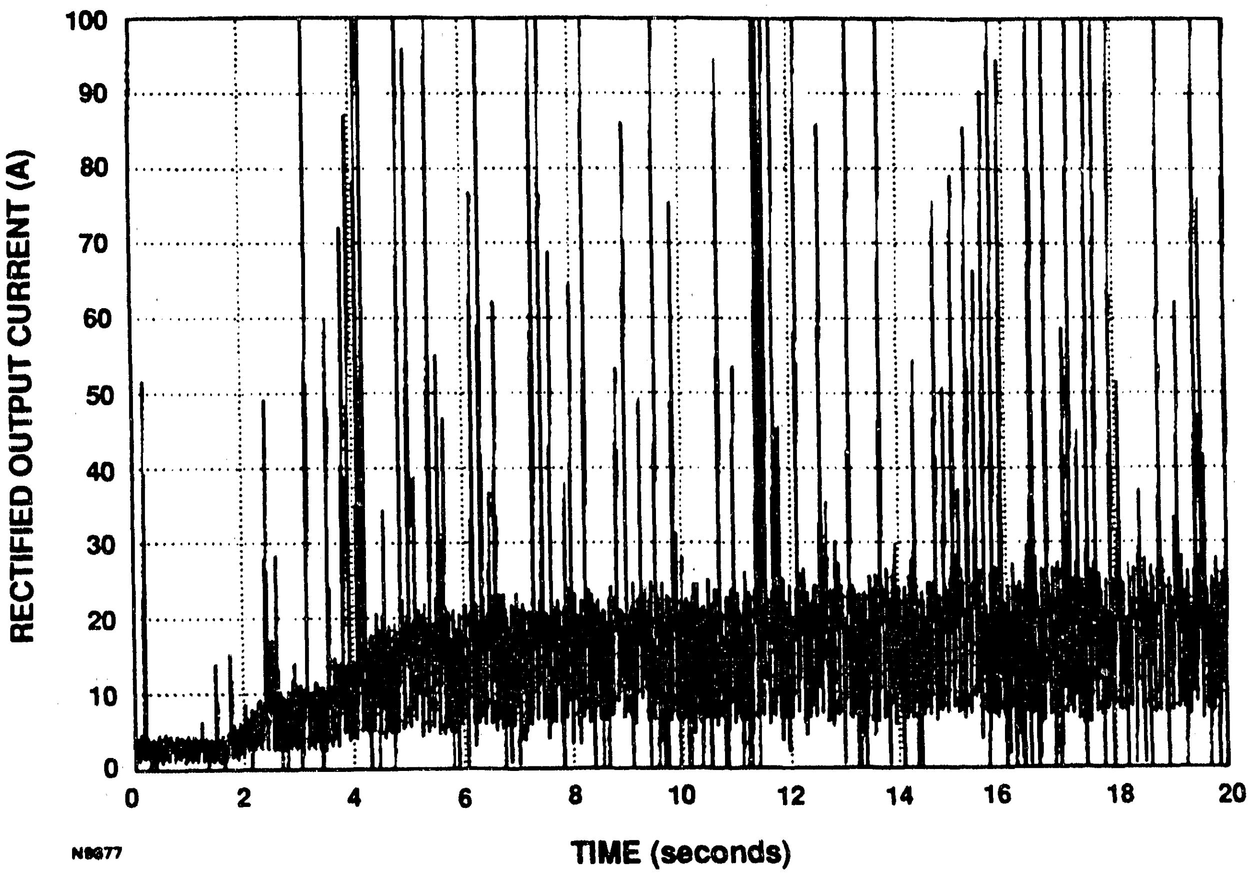

Figure 34 Rectified Output (Secondary) Current Over a 20 sec Period After the Test Start

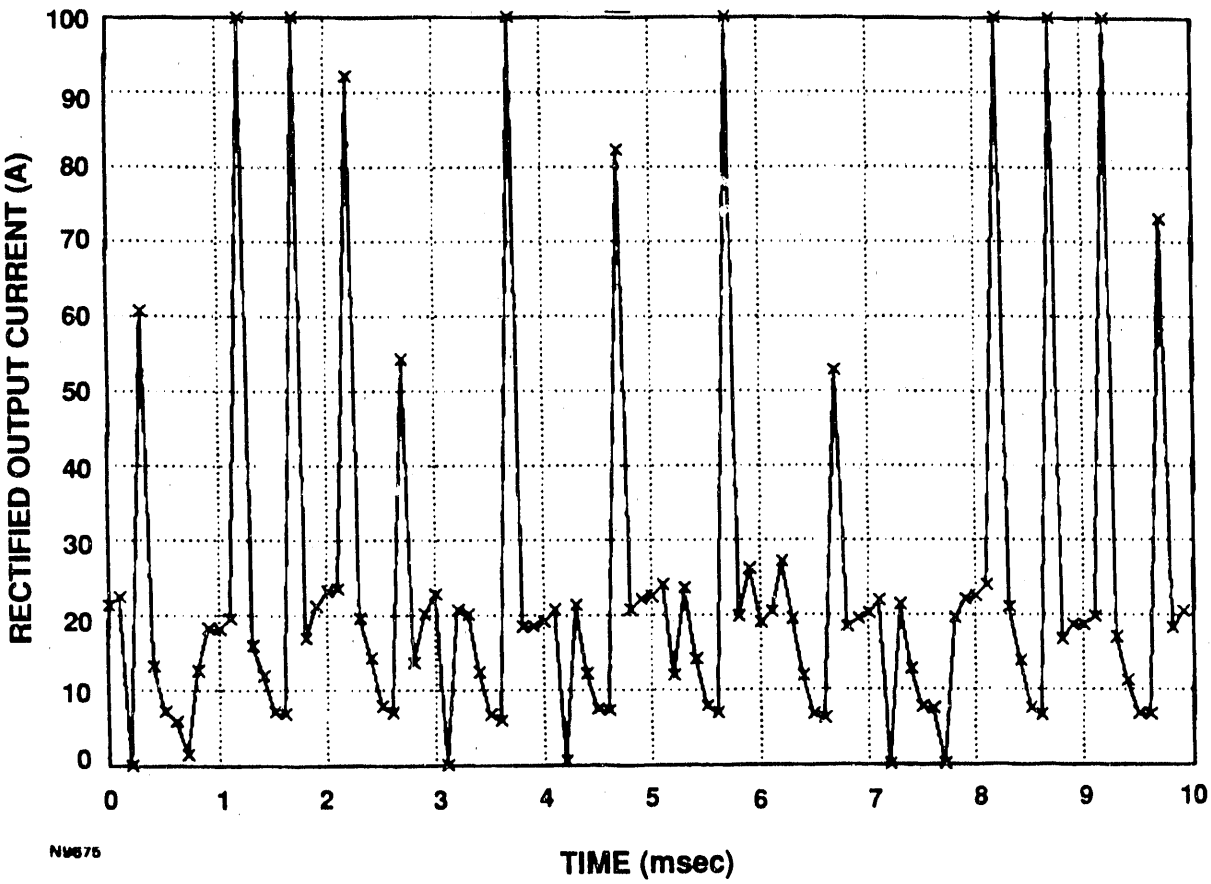

Figure 35 Rectified Output (Secondary) Current Over a 10 msec Period 10 sec into the Test

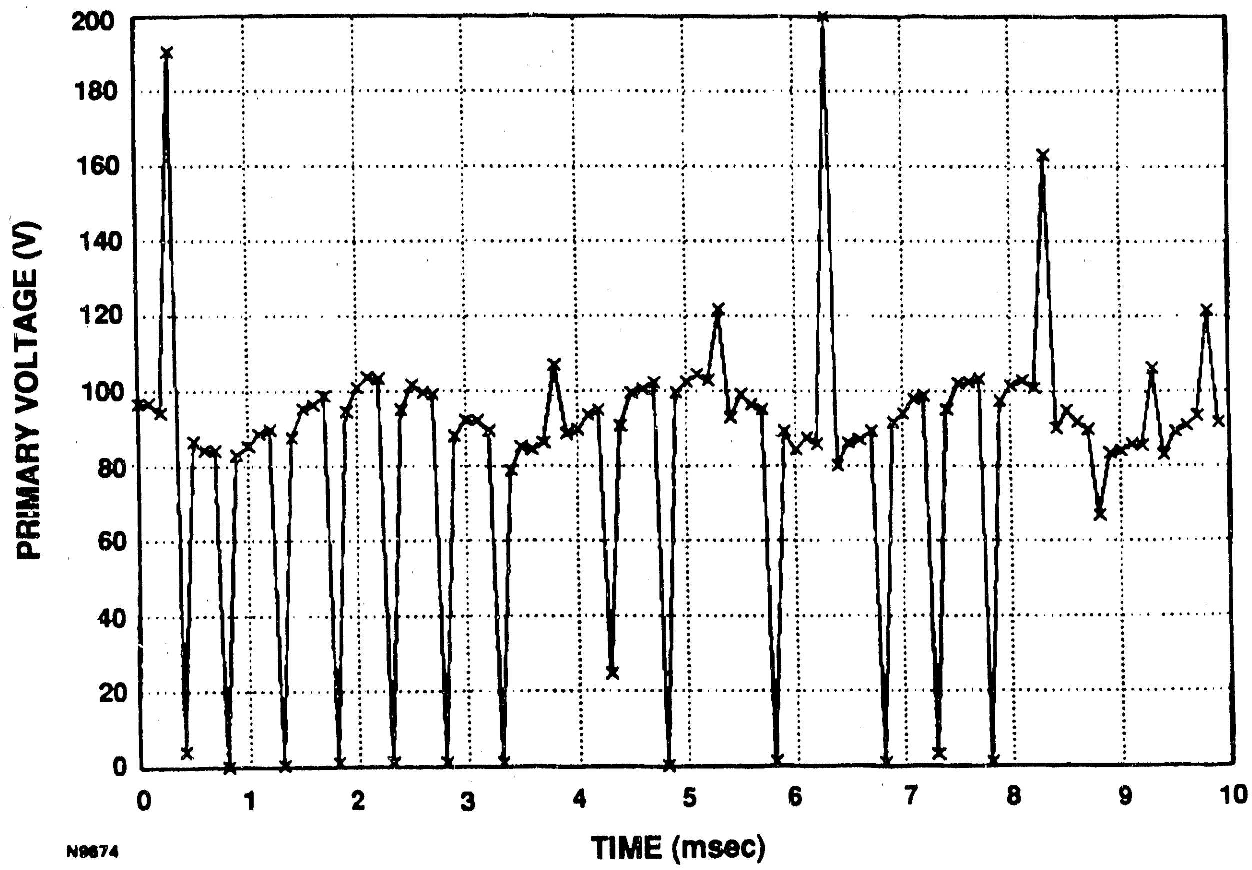

Figure 36 Primary Voltage Over a 10 msec Period 10 sec into the Test

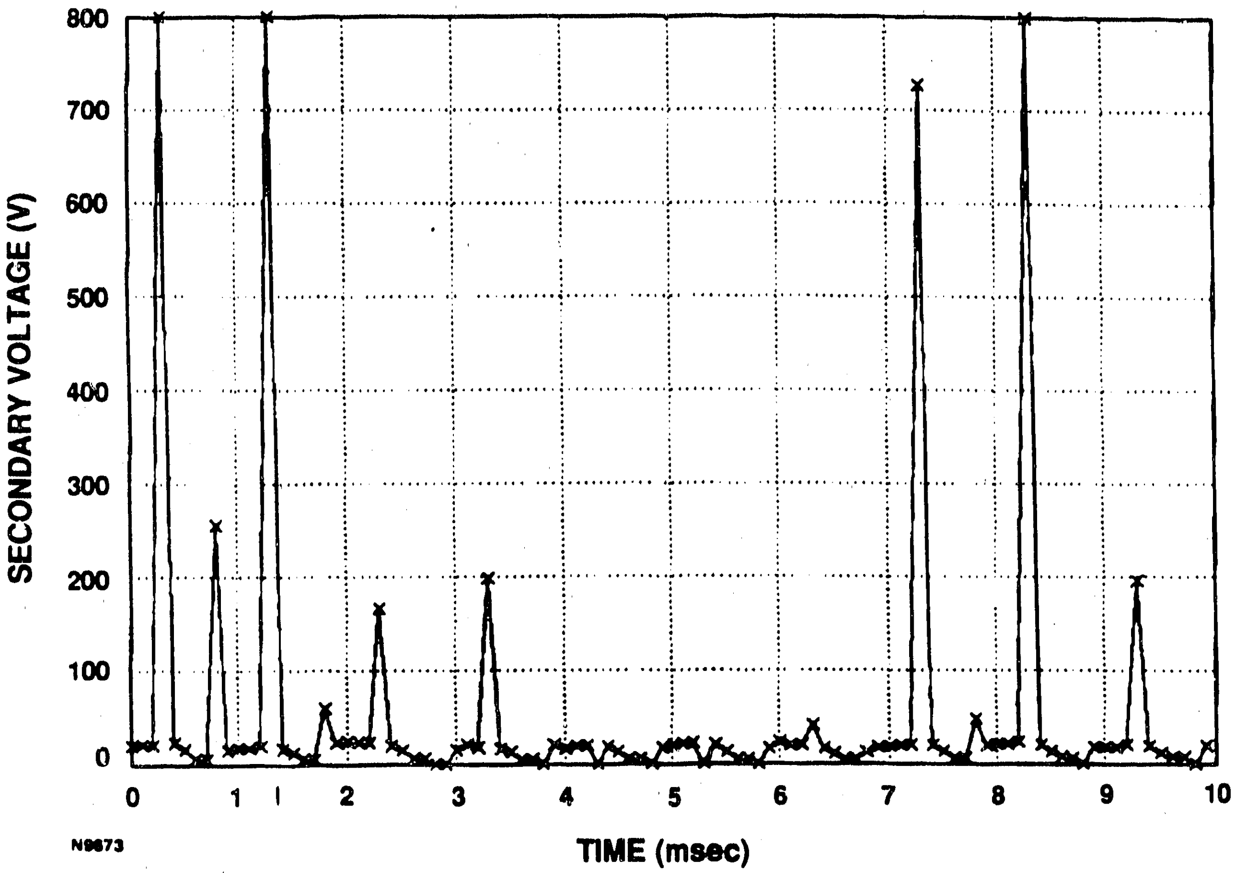

Figure 37 Secondary Voltage Over a 10 msec Period 10 sec into the Test

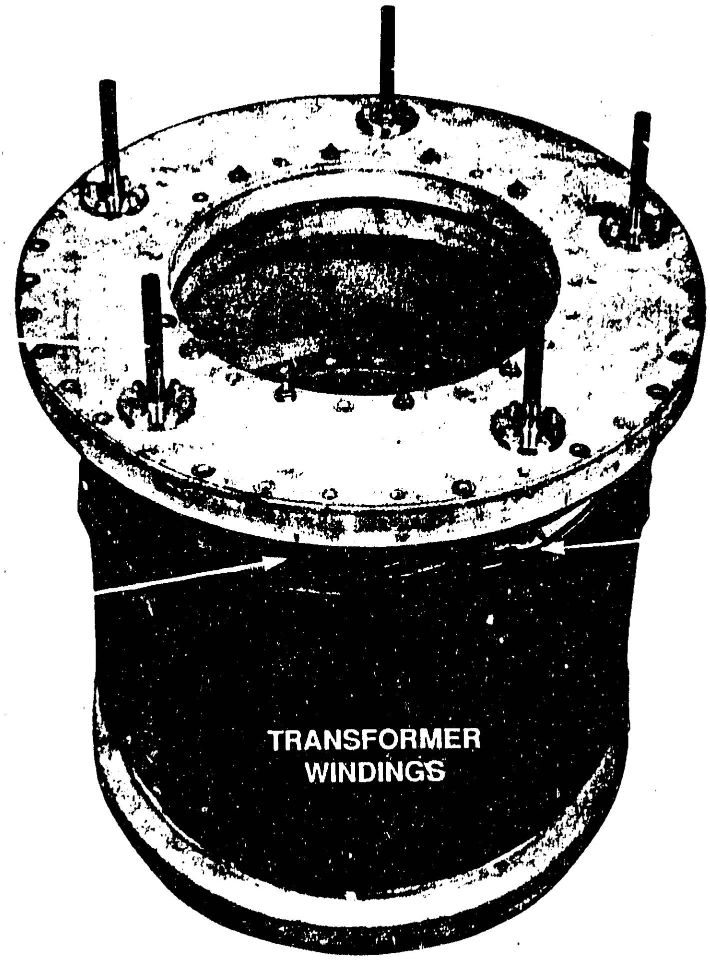

Figure 38 Post Test Condition of the Transformer Windings

7.0 DISCUSSION OF THE RESULTS

During low power testing the transformer functioned as designed. The design primary to secondary voltage ratio was ten. The achieved ratio, depending on the load, was approximately 9.6. However, both the primary and secondary self and mutual inductances fell approximately 30 percent below the design value. This shortfall was investigated by using several separately wound coils with a different number of turns and different diameter coils. The predicted and measured inductances agreed within ten percent.

The effect of frequency on the measured inductances as well as the winding temperature (room temperature to LN_2 temperature) was investigated to determine if multidistribution of current within the foil type conductor was the cause. This was suspected to cause the observed drop off of the inductances with increasing frequency (up to 10 kHz) and decreasing temperature. A literature search revealed that the concept of "effective frequency" advanced by Graneau[8] may be applicable. The effective or generalized frequency (λ) determines the current distribution in the conductor and is given by

$$\lambda = x^2 \, (\sigma_x/\sigma)\omega, \qquad (19)$$

where x is a scaling coil size dependent factor, σ_x is the material conductivity at other than room temperature, σ is the material conductivity at room temperature and ω is angular frequency of the applied voltage.

Thus, as the metal conductivity increases with decreasing temperature, the normalized frequency increases and, the current distribution becomes more nonuniform which causes the self inductance to decrease. A qualitative schematic of the situation is shown in Figure 39. To mitigate this effect, the secondary to primary windings must be interleafed. This forces uniform current distribution in both the primary and the secondary conductor, and the number of turns must be minimized to minimize the leakage inductances. The only way to minimize the number of primary turns for a given desired self inductance is to use magnetic core materials. Thus, as previously suggested,

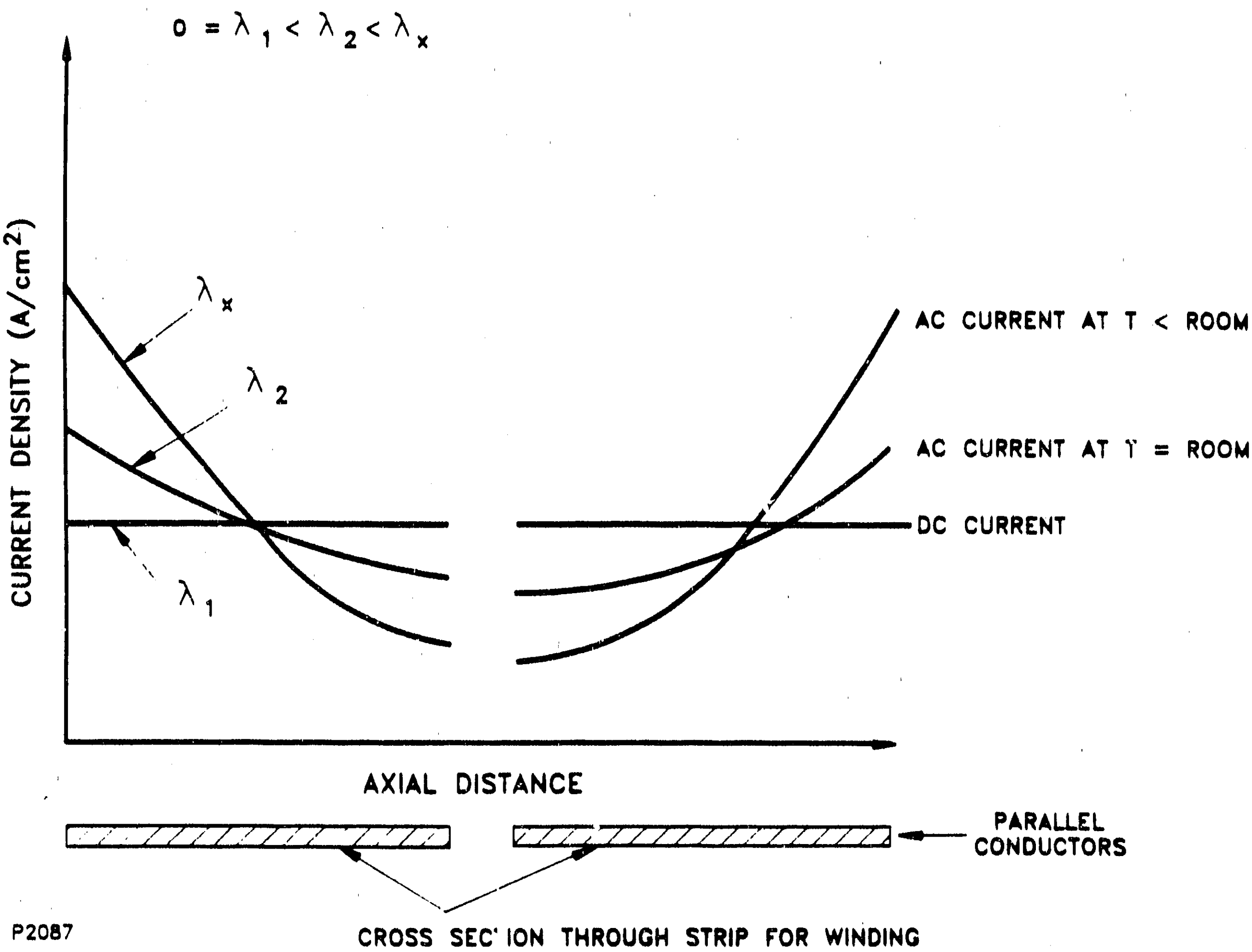

Figure 39 Increasing Material Conductivity (Lowering Temperature) Causes Increasing Nonuniformity of Current Distribution Within the Conductor